

AD-9190 497

PERFORMANCE OPTIMIZATION OF A CRUISE MISSILE USING
DYNAMIC-STALL INDUCED. (U) AIR FORCE INST OF TECH
WRIGHT-PATTERSON AFB OH SCHOOL OF ENGI. W J DARDIS

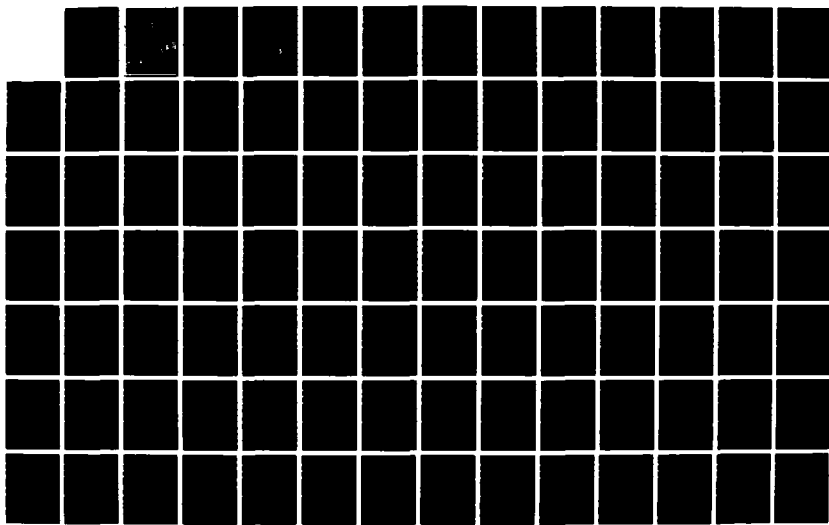
1/2

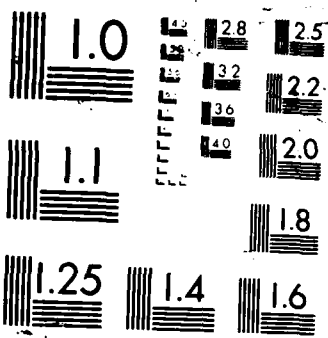
UNCLASSIFIED

SEP 87 AFIT/GAE/MA/875-1

F/G 16/2.1

NL





DTIC FILE COPY

AD-A190 497



AIR UNIVERSITY
UNITED STATES AIR FORCE

PERFORMANCE OPTIMIZATION OF A CRUISE MISSILE
USING DYNAMIC-STALL INDUCED
LIFT AUGMENTATION

William J. Dardis III
AFIT/GAE/AA/87S-1

DTIC
SELECTED
MAR 03 1988

S
E
T
E
M
B
R

Q
D

SCHOOL OF ENGINEERING

DISTRIBUTION STATEMENT A
Approved for public release
Distribution Unlimited

WRIGHT-PATTERSON AIR FORCE BASE, OHIO

88 3 01 142

AFIT/GAE/AA/87S-1

PERFORMANCE OPTIMIZATION OF A CRUISE MISSILE
USING DYNAMIC-STALL INDUCED
LIFT AUGMENTATION

THESIS

Presented to the Faculty of the School of Engineering
of the Air Force Institute of Technology
Air University
In Partial Fulfillment of the
Requirements for the Degree of
Master of Science in Aeronautical Engineering



William J. Dardis III, B.S.

September 1987

Approved for public release; distribution unlimited

Accession For	
NTIS	CRA&I <input checked="" type="checkbox"/>
DTIC	TAB <input type="checkbox"/>
Unpublished	
Justification	
By	
Det. Director	
Av. Facility Codes	
Funding Source	
DTIC	Special
A-1	

AFIT/GAE/AA/87S-1

6

PERFORMANCE OPTIMIZATION OF A CRUISE MISSILE
USING DYNAMIC-STALL INDUCED
LIFT AUGMENTATION

William J. Dardis III
AFIT/GAE/AA/87S-1

DTIC
SELECTED
MAR 03 1988
S D
D

Approved for public release; distribution unlimited

Acknowledgements

I would like to express my sincerest thanks to the many people over the past year who have helped to make this research effort possible. I would like to thank Lt. Col. Eric Jumper, my advisor, whose patients, enthusiasm, and constant vigilance helped to provide the motivation I needed to stick with and complete this investigation. I would also like to thank Bruce Fox, Mark Fellows, Joe Manter, Jim Engle, Jerry Forner, Dick Dyer, and Dorothy Arbiter of ASD/ENFTA for their help, patience and expert advice throughout this effort. I especially would like to thank Bruce Fox, who was always available to offer assistance when I was confronted with computer model difficulties, and Joe Manter, who was always willing to give me the time at work needed to complete this investigation. I would like to thank Maj. Hudson who, in the past month since Lt. Col. Jumper's absence, has provided valuable advice and assistance. Finally, I would like to express my deepest appreciation to the three (and very soon four) most important people in my life. Chris, Annie, and Patrick, thank you for the constant love, support, and patience that made all of this a reality.

Table of Contents

	Page
Acknowledgements	ii
List of Figures	v
List of Tables	vi
List of Symbols	ix
Abstract	xii
I. Introduction	1.1
Background	1.1
Objectives	1.9
II. Vehicle Design	2.1
Why A Cruise Missile	2.1
Baseline Vehicle	2.5
Augmented Lift Vehicles	2.5
Design Limitations	2.17
III. Range, Trajectory, and Mission Elements	3.1
Range	3.1
Trajectory Equations	3.4
Mission Elements	3.8
Complete Missions	3.11
IV. Results and Discussion	4.1
Straight-and-Level Range	4.1
Mission Elements For Terrain Following	4.7
Missions	4.18
V. Conclusions and Recommendations	5.1
Bibliography	BIB.1
Appendix A: Vehicle Drag Polar Development	A.1

Appendix B: Critical Mach Number Considerations	B.1
Appendix C: Sample Input and Output for Programs NSEGII and IIID	C.1
Appendix D: Remainder of Tabulated Results	D.1
Vita	V.1

List of Figures

Figure		Page
1.1.	Results From Dimmick [6:Fig 40] for a Non-Dimensional Pitch Rate of 0.025	1.4
1.2	Results from McCalister, Carr, and McCroskey [13:Fig 55e] for a Sinusoidal Pitch Rate of $\alpha = 15 + 10 \sin \omega t$, $k = 0.150$	1.5
1.3	Results from Stephen [14:Fig 30] for an $\alpha_{ND\ up} = 0.0142$, $\alpha_{ND\ dn} = 0.1250$ Showing a 1.14 increase in Time Averaged Dynamic Lift . .	1.7
2.1	A Typical Drag Polar Displaying the Concept of the "Oversized" Cruise Missile Wing	2.2
2.2	Baseline Vehicle Configuration	2.6
2.3	Engine Thrust vs. SFC at Sea Level	2.7
2.4	Engine Thrust vs. SFC at 10000 ft Altitude	2.8
2.5	Reduced Wing Area Criteria for the Dynamic-Lift Vehicles	2.14
2.6	Limit of Span Reduction to Decrease Drag. From Kohlman [24:Fig 2]	2.18
2.7	Drag Polars of Four Vehicles Based on the Same Reference Area (13 Square Ft)	2.20
3.1	Force Diagram for a Typical Aircraft	3.5
3.2	Typical Cruise-Missile-Type Missions	3.13
4.1	Range at Optimum Mach Number (Sea Level)	4.2
4.2	Range at Optimum Mach Number (H = 10000 ft)	4.3
4.3	Thrust and SFC for the Four Vehicles Through a Typical Mission ($M_0 = 0.5$ at Sea Level)	4.4

Figure	Page
4.4 Flight Path Angle vs. Time for a $C_{L_{max}}$ Climb	4.8
4.5 Altitude vs. Time for a $C_{L_{max}}$ Climb	4.9
4.6 Vehicle Weight vs. Achievable Flight Path Angle	4.11
4.7 Altitude vs. Downrange for a Pull Out from $\gamma = -90^\circ$ at Max Thrust	4.12
4.8 Altitude vs. Downrange for a Pull Out from $\gamma = -45^\circ$ at Max Thrust	4.13
4.9 Altitude vs. Downrange for a Pull Out from $\gamma = -30^\circ$ at Max Thrust	4.14
4.10 Altitude vs. Downrange for a Pull Out from $\gamma = -15^\circ$ at Max Thrust	4.15
4.11 Time to Pull Out vs. Initial Flight Path Angle at Max Thrust	4.16
4.12 Pull-Over Maneuver from $\gamma = +45^\circ$ to -45° . Weight = 2000 lbs	4.18
4.13 Specific Excess Power vs. Time for the Pull-Over Maneuver in Figure 4.12	4.20
4.14 Range vs. Vehicle Weight for Mission Planning	4.22
4.15 Average Fuel Weight Loss vs. Distance Covered During the Terrain Following Mode	4.24
4.16 Vehicle Trajectories for Mission 1	4.25
4.17 Vehicle Trajectories for Mission 2	4.28
B.1 Critical Mach Number For the 0015 Airfoil During Dynamic-Lift Operation	B.5

List of Tables

Table		Page
2.1	Comparison of Four Vehicle Configurations	2.19
4.1	Percent Change in Range With the Baseline Vehicle for the Three Optimization Techniques	4.6
4.2	Mission 1 - Range and Time Above Sea Level for All Four Vehicles	4.26
4.3	Mission 2 - Range and Time Above Sea Level for All Four Vehicles	4.29
D.1	Vehicle Range For Mach Number Equal to 0.5 at Sea Level With the Baseline Engine	D.2
D.2	Vehicle Range Optimized for Cruise Mach Number at Sea Level With the Baseline Engine	D.3
D.3	Vehicle Range Optimized for Cruise Mach Number at 10000 ft Altitude With the Baseline Engine	D.4
D.4	Vehicle Range for Optimum Dynamic Vehicle Engine Thrust Characteristics at Mach Number Equal to 0.5 at Sea Level	D.5
D.5	Maximum Lift Coefficient Climb at Weight = 3000 lbs	D.6
D.6	Maximum Lift Coefficient Climb at Weight = 2000 lbs	D.7
D.7	Maximum Lift Coefficient Climb at Weight = 1000 lbs	D.8
D.8	Pull Out of Dive Maneuver for All Four Vehicles at Weight = 3000 lbs	D.9
D.9	Pull Out of Dive Maneuver for All Four Vehicles at Weight = 2000 lbs	D.10

Table		Page
D.10	Pull Out of Dive Maneuver for All Four Vehicles at Weight = 1000 lbs	D.11
D.11	Effect of Thrust on Pull-Over Capability for a Vehicle Weight of 3000 lbs at $\gamma = -90^\circ$, and an Initial Mach Number of 0.0	D.12
D.12	Mission 1 - Baseline Vehicle Traversing the First Mountain	D.13
D.13	Mission 1 - Vehicle 1 Traversing the First Mountain	D.14
D.14	Mission 1 - Vehicle 2 Traversing the First Mountain	D.15
D.15	Mission 1 - Vehicle 3 Traversing the First Mountain	D.16
D.16	Mission 1 - Fuel Loss Estimate For the Terrain Following Portion of the Mission	D.17
D.17	Mission 2 - Baseline Vehicle Traversing the First Mountain	D.18
D.18	Mission 2 - Vehicle 1 Traversing the First Mountain	D.19
D.19	Mission 2 - Vehicle 2 Traversing The First Mountain	D.20
D.20	Mission 2 - Vehicle 3 Traversing the First Mountain	D.21
D.21	Mission 2 - Fuel Loss Estimate For the Terrain Following Portion of the Mission	D.22

List of Symbols

AR	aspect ratio
b	wing span
c	wing chord
C_C	chord-force moment coefficient
C_D	drag coefficient
C_{D0}	drag coefficient at zero lift
C_f	turbulent flat plat skin friction coefficient
C_L	lift coefficient
c_l	section lift coefficient
C_M	pitching moment coefficient
C_N	chord normal aerodynamic coefficient
C_p	pressure coefficient
D	drag
d	diameter or vehicle body diameter
D_p	wing profile drag
D_w	total wing drag
e	wing efficiency factor
F_N	net propulsive force
H	altitude
K	drag due to lift factor
k	equivalent sand roughness

K'	inviscid drag due to lift factor
K''	viscous drag due to lift factor
L	lift
L_p	airfoil thickness location factor
M	Mach Number or pitching moment
m_0	section lift curve slope
n	longitudinal load factor
P	ratio of parasite to total drag
P_s	specific excess power
q	dynamic pressure
R	lifting surface correlation factor
S	wing reference area
s	distance
S_{BD}	cross-sectional area of the vehicle body
SFC	specific fuel consumption
S_s	total body wetted area
S_{wetw}	wing wetted area
t	time or airfoil max thickness
V	freestream velocity
W	vehicle weight
Y	horizontal distance
$\dot{\alpha}$	angle of attack angular rate

$\dot{\alpha}_{ND}$ non-dimensional angular rate

γ flight path angle

subscripts

max maximum value

dyn refers to dynamic lift vehicles or dynamic value

st static value

B refers to baseline vehicle

R some reference condition

cg center of gravity

BD vehicle body

x local airfoil site

∞ freestream

Abstract

An investigation was conducted to study the possible performance benefits of using the augmented lift produced by dynamic-stall-type airfoil motions to a cruise-missile-type aircraft in terms of range, climb capability, and susceptibility to threat. A baseline cruise-missile-type aircraft is defined and compared to three modified versions with augmented lift capability. The wings for the three dynamic-lift vehicles are sized to produce the same maximum lift coefficient, while operating dynamically, as the maximum usable lift coefficient (0.8 times maximum lift coefficient) of the baseline aircraft. By resizing the wing through chord reduction, increases in straight-and-level range of 20 to 25% are found along with improvements in climb, pull over terrain, and pull up from a dive, capability. Moderate improvements in performance are found for the same aspect ratio vehicle. The vehicle resized by span reduction consistently under-performed all vehicles except in some examples of pull out to level flight. Two typical cruise-missile-type missions were chosen and the trajectories of the four vehicles were modeled. Minimum time above a reference altitude was determined for the two missions as a representative measure of susceptibility to threat.

PERFORMANCE OPTIMIZATION OF A CRUISE
MISSILE USING DYNAMIC-STALL INDUCED
LIFT AUGMENTATION

I. Introduction

Background

Dynamic stall is an unsteady phenomenon that occurs when an airfoil passes through (from below) its static-stall angle of attack with some rate. As the airfoil passes through the static-stall angle of attack, stall is delayed until a higher angle of attack is reached, the so-called dynamic-stall angle of attack. During this process, the lift coefficient of the airfoil is increased beyond the static maximum value of lift. The possible exploitation of this dynamically-increased maximum lift is the purpose of this investigation.

The first published record of dynamic stall was reported by Max Von Kramer after pilots noted increased lift while flying in turbulent air [1]. Since that time, dynamic-stall-like phenomena has been noted in a range of aerodynamic applications from the effect of periodic rotational motions on compressor blades [2], to the effect of retreating blade stall in helicopter rotors [3]. Kramer developed an empirical relationship between dynamic and static lift coefficient for an airfoil undergoing a constant rate

of change of angle of attack

$$C_{L_{\max \text{ dyn}}} = C_{L_{\max \text{ st}}} + (0.036 \dot{\alpha}) / V \quad (1.1)$$

Deekens and Keubler [4] used flow visualization and an assumed connection between quarter-chord separation and stall to arrive at a similar relationship which was later verified by Daley [5]. Their relationship, however, showed a stronger effect on dynamic $C_{L_{\max}}$ due to the non-dimensionalized pitch rate term $c \dot{\alpha} / V$ (i.e. a larger lift curve slope). Deekens' and Keubler's equation has been written here in terms of radians and multiplied by the $2\pi / \text{radian}$ slope curve of classical theory so it may be compared to Equation 1.1

$$C_{L_{\max \text{ dyn}}} = C_{L_{\max \text{ st}}} + (0.264 c \dot{\alpha}) / V \quad (1.2)$$

The difference between these two equations, as explained by Dimmick [6], may be due to the different experimental approaches by Kramer and Deekens and Keubler. While both dealt with constant- $\dot{\alpha}$ experiments, Kramer's experimental airfoils were fixed in inertial space with a varying flowfield. Deekens and Keubler used a rotating airfoil in a constant velocity flowfield. Dimmick points out that the analytical treatment of the flowfield over the airfoil for the later

case must be accomplished using an accelerating control volume.

Lawrence [7], Tupper [8], and Allaire [9] increased the understanding of the dynamic stall event through various analytical approaches while Schreck [10] and Dimmick [6] added to the available experimental database for constant- $\dot{\alpha}$ pitching airfoils. Recent studies by Jumper, Schreck, and Dimmick [11], [12], have shown that a doubling of static $C_{L_{max}}$ can easily be obtained with relatively small pitch rates (i.e. $\dot{\alpha}_{ND} \leq 0.02$).

To exploit the dynamic-stall event for lift augmentation, some measure of the dynamic induced lift must be maintained over time without a large penalty associated with the increases in drag and pitching moment. As shown in a sample of Dimmick's experimental work (see Figure 1.1), lift increases through a rotation of the airfoil but a point is reached where a large negative pitching moment occurs along with a large increase in drag. While constant- $\dot{\alpha}$ experiments have been useful in understanding some of the mechanisms at work in dynamic-stall, any hope of time-averaged lift augmentation over an extended and useful period of time will depend on some kind of periodic motion.

Experiments performed by McAlister, Carr, and McCroskey [13] also demonstrated increases in chord-normal aerodynamic coefficients, C_N , as high as 2.33 times $C_{N_{static}}$ using sinusoidal oscillations of a 0012 airfoil about an average angle of attack (Figure 1.2). However, the time-averaged or integrated C_N for a period of motion (crossed-hatched region of Figure 1.2) is not increased above $C_{N_{max static}}$. Furthermore, based on these data alone, the corres-

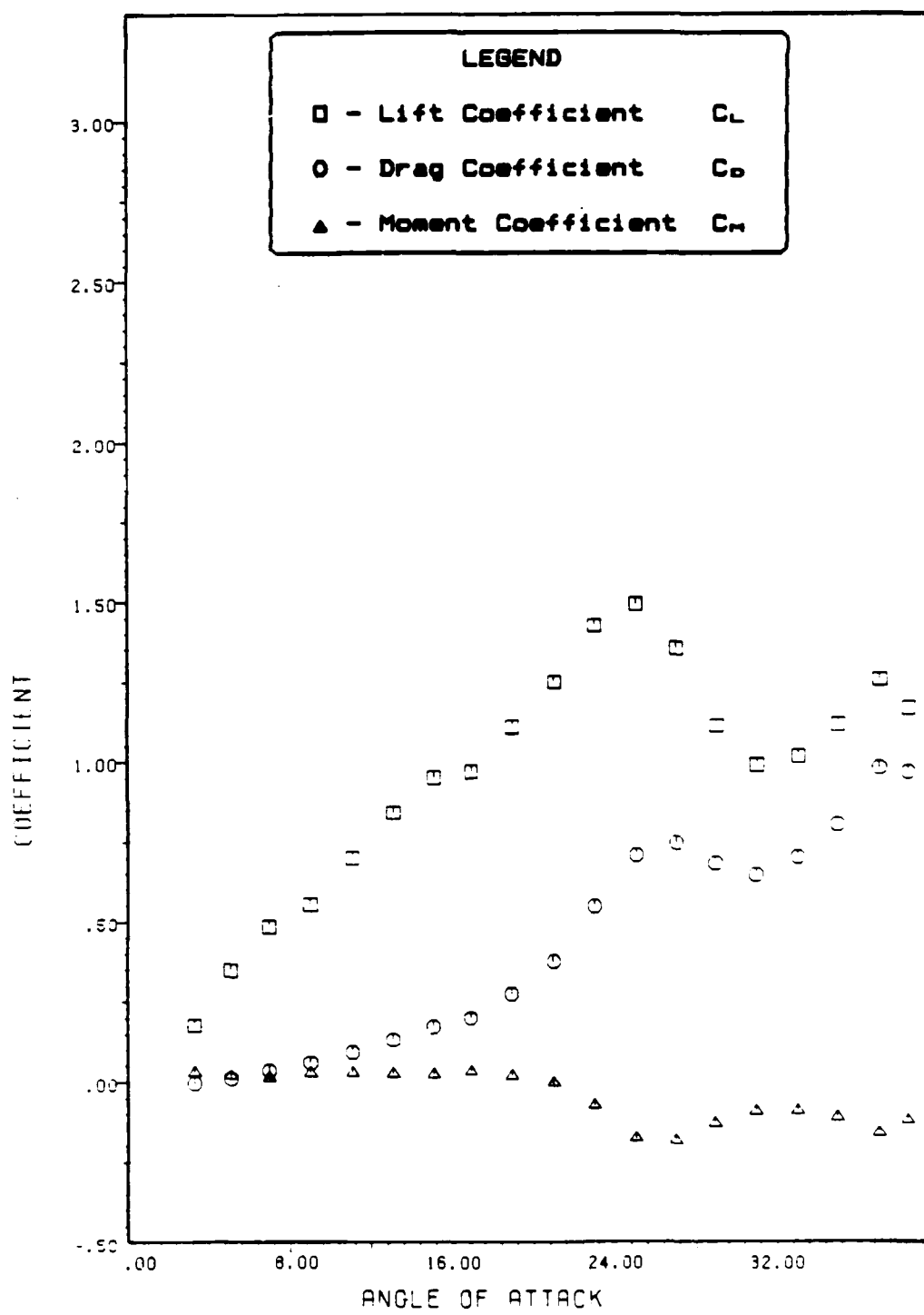


Figure 1.1. Results from Dimmick [6:Fig 40] for a Non-Dimensional Pitch Rate of 0.025

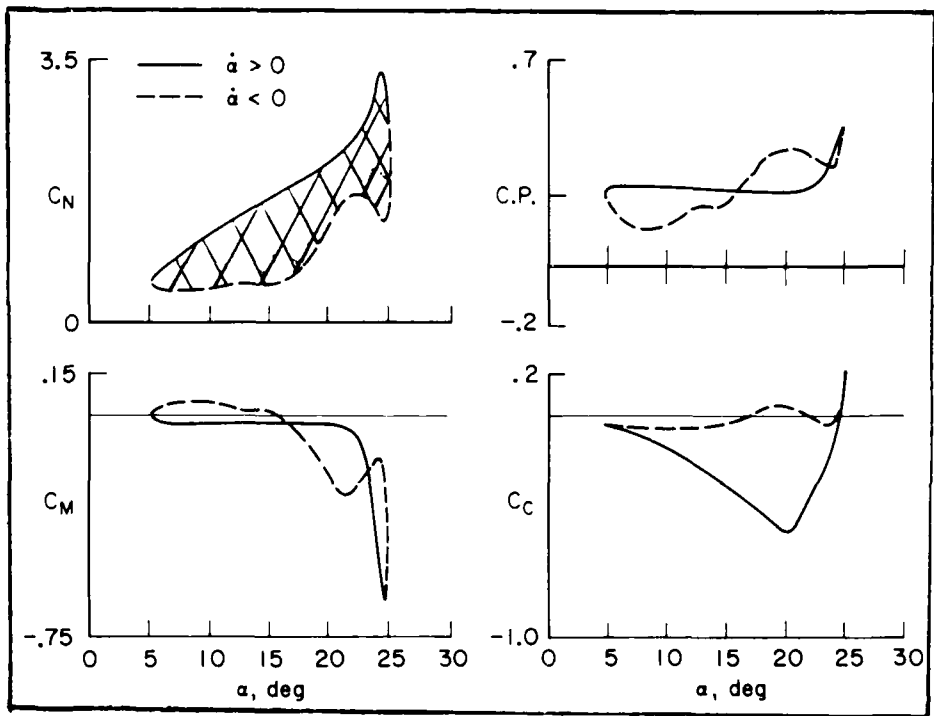


Figure 1.2. Results from McCalister, Carr, and McCroskey [13:Fig 55e] for a Sinusoidal Motion of
 $\alpha = 15^\circ + 10^\circ \sin \omega t$, $\kappa = 0.150$

ponding values of pitching-moment coefficient, C_M , and chord-force moment, C_C , are sufficiently large to imply precluding the use of sinusoidal motions for lift augmentation.

With an increased understanding of the dynamic-stall event provided by studies of the constant- $\dot{\alpha}$ motion, and the promise of potentially large average lift values, Stephen [14] began a new study to investigate other types of airfoil periodic motions where time-averaged lift coefficient might exceed $C_l \text{max static}$. With a series of periodic constant- $\dot{\alpha}$, ramp-up, snap-down motions, Stephen demonstrated, in one instance, that an average lift coefficient of 1.114 times the steady $C_l \text{max}$ could be achieved with only a slight increase in drag and pitching moment (Figure 1.3). Although this value of lift coefficient is short of what might be hoped for, Stephen did discover a periodic motion where drag and pitching moment were only slightly effected. Because of experimental difficulties, Stephen was not able to systematically explore such motions further, but based upon these results, his study indicated that higher average values of lift coefficient may be attainable.

Another important finding suggested by Stephen's work is that the leading-edge vortex formation and shedding, which has been considered the driving mechanism in dynamic lift augmentation [3, 13, 15], may not be as important as earlier believed. Stephen's results appear to indicate that sustained average lift values can be achieved without the formation of the leading-edge vortex during the upward movement in the periodic motion. Further, suppression of such leading-edge vortex formation is probably responsible for avoiding the detrimental

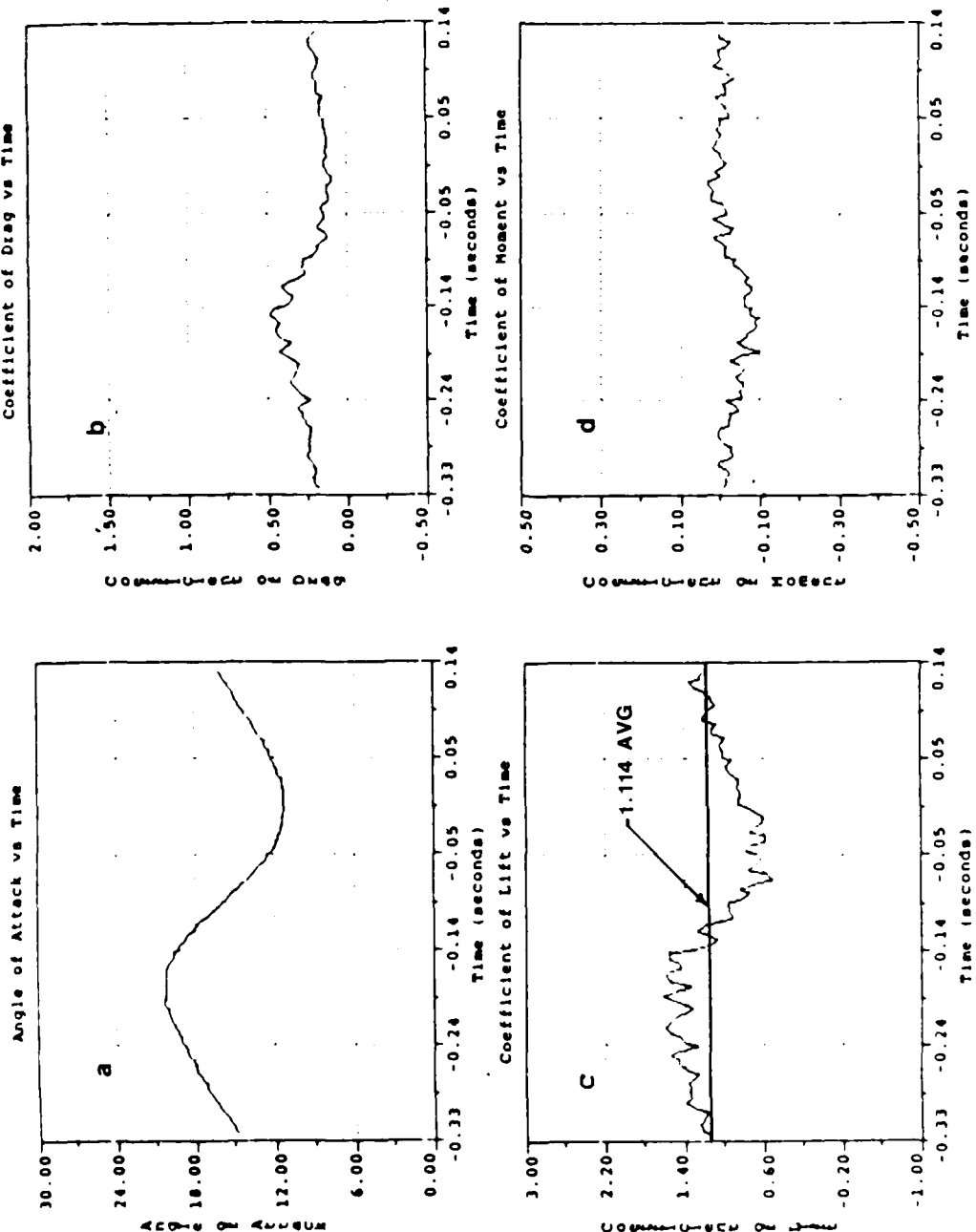


Figure 1.3. Results from Stephen [14:Fig 30] for an $\alpha_{NDup} = .0142$, $\alpha_{NDdown} = .0250$ Showing a 1.114 Increase in Time Averaged Dynamic Lift

drag and moment effects evidenced in previous studies. The results suggest that the primary mechanism in delaying upper surface separation may be related to the combined effect of the Moore-Rott-Sears separation criteria for a wall moving in the direction of the flow discussed by Williams [22], Lawrence's [7] proposed mass ingestion through the "boundary-layer control volume", and the effect of the unsteady wake [19].

Based upon the results of Stephen and his predecessors, this study was initiated to explore the potential performance benefits of dynamic-stall-induced augmented lift on an aircraft. Although there are acknowledgements to the potential uses of dynamic stall produced lift by Ashley [16], Hamilton, et. al. [17], and Lang and Francis [18], most of the interest has been in increasing the maneuverability of fighter aircraft. Lang and Francis [18] have done a simple study showing increased turn rate capability with the benefits of dynamic-stall-induced lift, but their interest has been centered around the characteristics and benefits of conventional fighter aircraft in transient maneuvers. The general approach of this study is to consider the benefits of unsteady, augmented lift applied to a lower-risk-mission aircraft (i.e. a cruise-missile-type vehicle) where the wing is decoupled from the fuselage about the transverse or pitch axis.

Objectives

The objectives of this investigation are to study the possible performance benefits of using the augmented lift produced by dynamic-stall-type airfoil motions to a cruise-missile-type aircraft in terms of range, climb capability, and susceptibility to threat. A baseline cruise-missile-type aircraft is defined and compared to three modified versions with augmented lift capability. The results are then used to "optimize" the range of each vehicle for a straight and level generic cruise-missile-type mission and the minimum time above a reference altitude for two terrain following missions.

II. Vehicle Design

This chapter describes the choice and preliminary design of four candidate vehicles for this study. Section 2 describes the design of a baseline cruise-missile-type vehicle. The remaining three aircraft configurations are described in Section 3. The later three vehicles will have dynamic-stall-induced lift identical to the maximum usable lift of the baseline vehicle thus allowing for different wing sizes. The wings for these three vehicles will be sized to produce the same $C_{L_{max}}$, while operating dynamically, as the maximum usable lift coefficient ($0.8 C_{L_{max\ st}}$) of the baseline vehicle.

Why a Cruise Missile

As was mentioned in Chapter 1, the cruise-missile-type vehicle was chosen as a candidate because of the low-risk-mission aspects of the vehicle. This vehicle and its mission requirements are considered low-risk as opposed to the risk associated with using conventional design practices to develop an expensive manned fighter-type vehicle. There is also another important reason why this vehicle is a good candidate for study. At first glance, it becomes apparent that the wing for a cruise-missile-type vehicle is small. However, the wing is "oversized" for the primary segment of the missile mission : straight-and-level cruise. To understand why this is true, observe a typical drag polar for this type vehicle (Figure 2.1). From Brequet's Range equation for a turbojet or turbofan [20] operating at a straight-

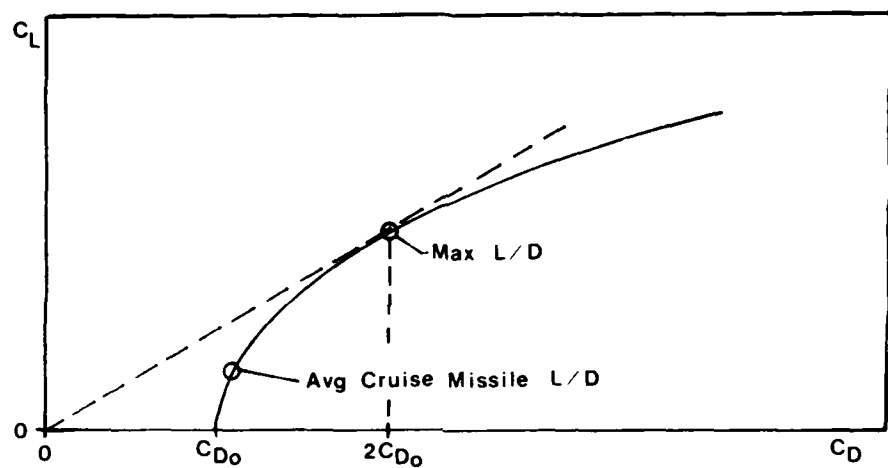


Figure 2.1. A Typical Drag Polar Displaying the Concept of the "Oversized" Cruise Missile Wing

and level cruise condition at constant velocity, V ,

$$R = (VL) / (SFC)(D) \ln (W_i / W_f) \quad (2.1)$$

we see that in order to maximize range, the average range parameter $[VL/(SFC)(D)]$ must be a maximum. This implies that L/D must be at or near a maximum value to provide for best vehicle range. The maximum L/D point on Figure 2.1 can be shown to occur at $2C_{D_0}$. If we look at the equation for the drag polar

$$C_D = C_{D_0} + KC_L^2 \quad (2.2)$$

dividing both sides of the equation by C_L

$$C_D / C_L = C_{D_0} / C_L + KC_L \quad (2.3)$$

we know then that C_D / C_L is a minimum (i.e. maximum L/D)

when

$$\frac{d(C_D / C_L)}{dC_L} = 0 = -C_{D_0} / C_L^2 + K \quad (2.4)$$

$$C_L^2_{\max L/D} = C_{D_0} / K \quad (2.5)$$

substituting equation 2.5 into equation 2.2 we indeed see that

$$C_{D_{\max L/D}} = C_{D_0} + KC_{D_0} / K = 2C_{D_0} \quad (2.6)$$

Typically, this class of vehicle cruises at a much lower value of average L/D for the cruise segment as represented in Figure 2.1. The reasons for this are not readily apparent until other segments of missile mission are examined. For terrain following, a cruise-missile-type vehicle must have a large available $C_{L_{\max}}$ for maneuvers. Therefore, the wing $C_{L_{\max}}$ is designed for maneuver considerations and is "oversized" for the cruise leg of most missions. If the vehicle had lift-augmentation capability (e.g. dynamic-stall-induced lift), a much smaller, efficient wing could be designed.

Baseline Vehicle

The small cruise-missile-type vehicle designed to serve as a baseline configuration for this study is shown in Figure 2.2. Rectangular planforms for the wing, vertical tail, and horizontal tail are used to simplify the design of the vehicle. The wing airfoil section was chosen to be the 0015 symmetrical airfoil to coincide with the airfoil section used in the previous experimental work by Stephen, Dimmick, and others mentioned in Chapter 1. The drag polar for this vehicle was found using the preliminary design methods outlined by Nicolai [20, 21] and is detailed in Appendix A. The baseline vehicle was designed to perform optimally at a Mach number of 0.5 at standard sea level conditions.

A baseline engine was chosen to provide sufficient thrust throughout the anticipated vehicle envelope. Figures 2.3 and 2.4 show the thrust versus specific fuel consumption, also known as engine power "hooks", developed for the baseline engine. The thrust characteristics of this engine are typical for a vehicle of this size.

Augmented Lift Vehicles

As was discussed in Chapter 1, Stephen found averaged increases in section lift coefficient of 1.114 times $C_{L_{max\ static}}$ with no appreciable increase in drag or moment coefficient. However, at the time this study was begun, Stephen's results were not completed. Therefore, based on Dimmick's results, a factor of 1.5 times $C_{L_{max\ static}}$ averaged over time was used as the dynamic-lift

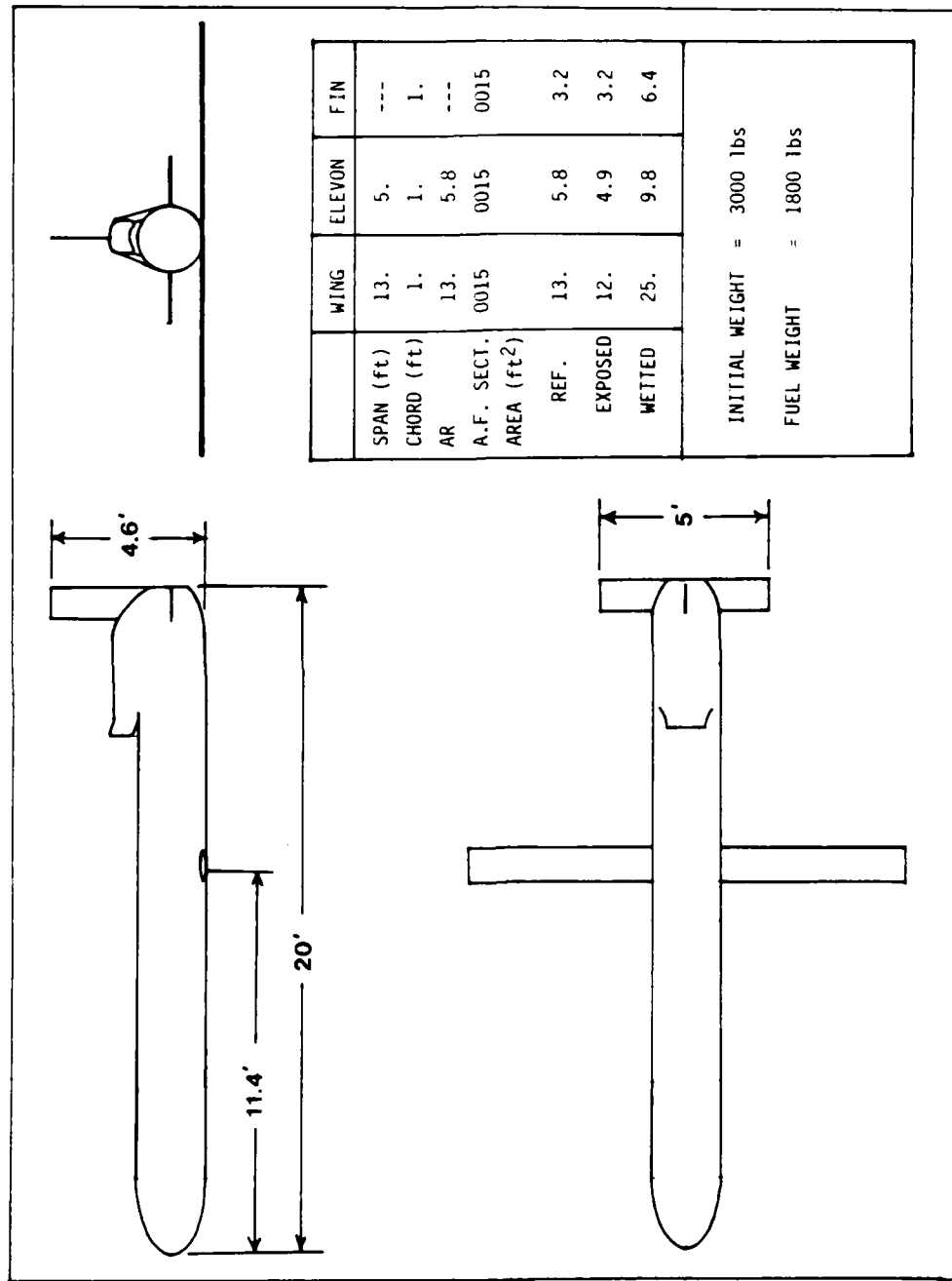


Figure 2.2. Baseline Vehicle Configuration

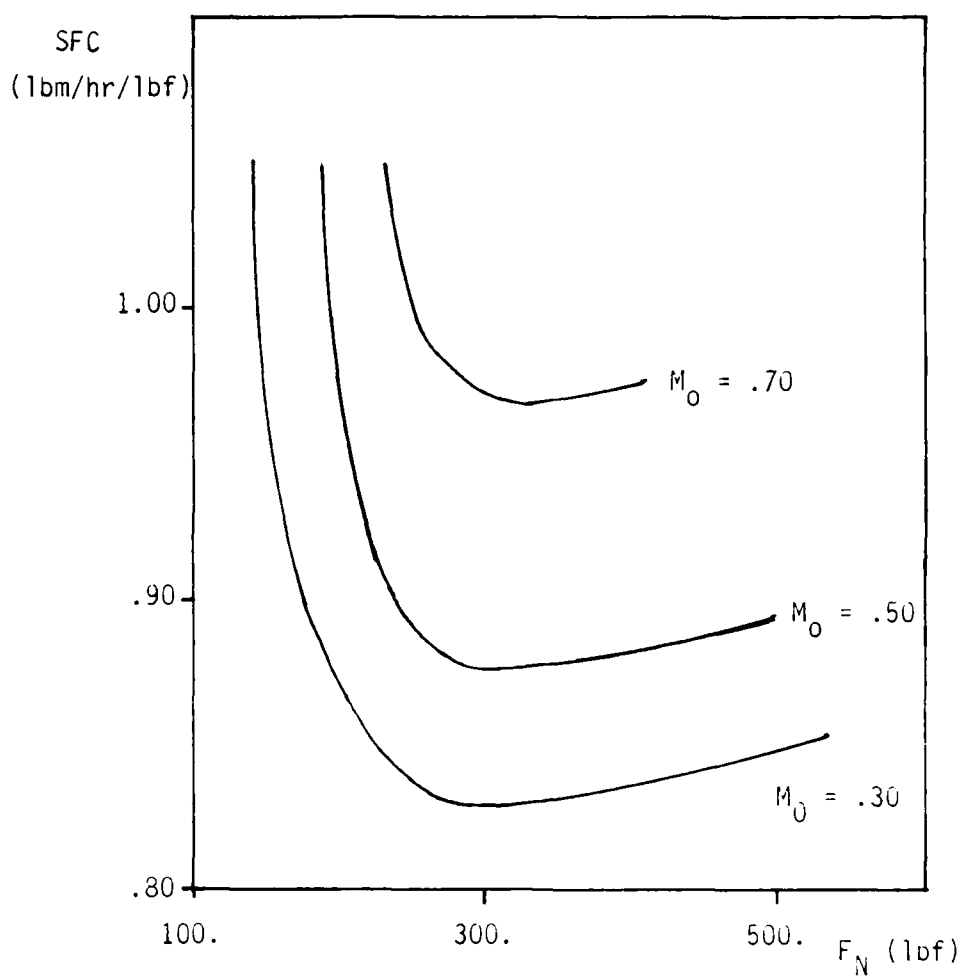


Figure 2.3. Engine Thrust vs. SFC at Sea Level

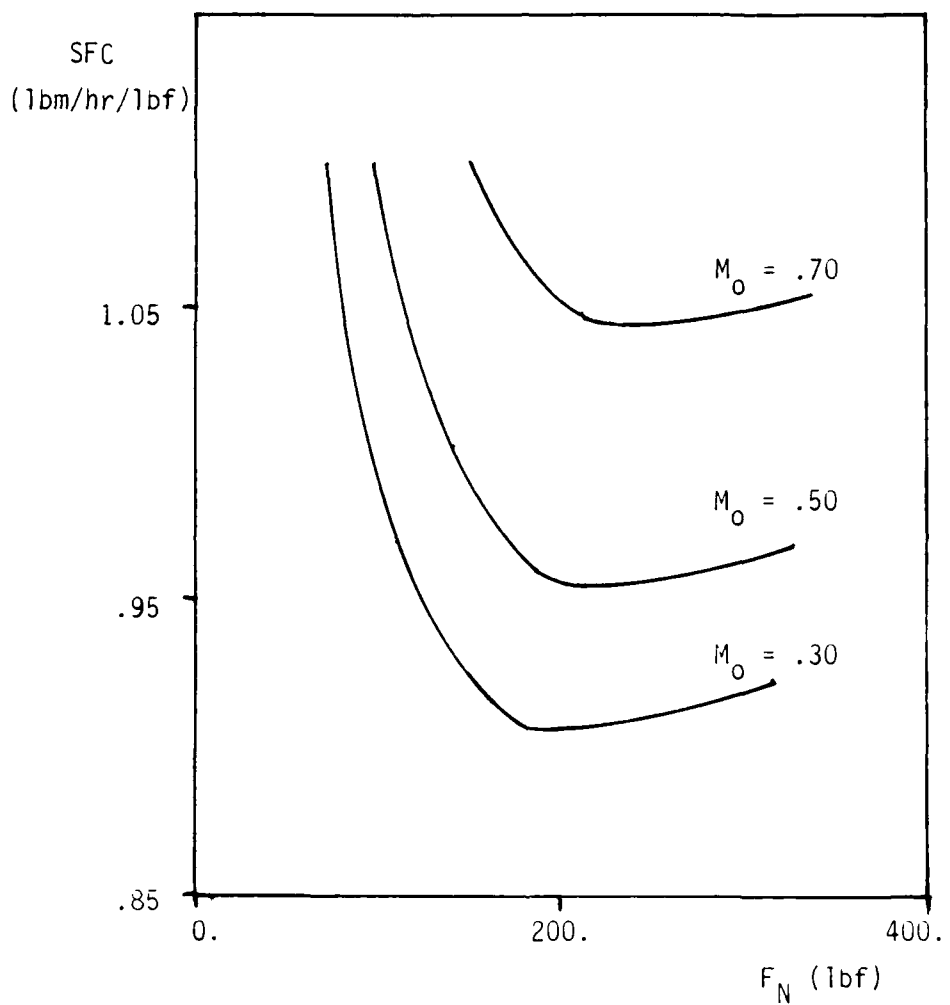


Figure 2.4. Engine Thrust vs. SFC at 10000 ft.
Altitude

criteria for this effort.

At this point, it is noteworthy to explain how the value of 1.5 was arrived at, keeping in mind that Stephen's work was not yet published. If we look at a sample of Dimmick's results presented in Figure 1.1 of Chapter 1 for a non-dimensional pitch rate, $\dot{\alpha}_{ND}$, of 0.025 where

$$\dot{\alpha}_{ND} = c\dot{\alpha} / 2V_\infty \quad (2.7)$$

a slight "knee" in the lift curve slope at the $\alpha = 20^\circ$ position is apparent. The general belief (later demonstrated by Stephen) was that if the upward motion of the airfoil was "clipped" or snapped down at this position, the airfoil would continue to generate lift up to or near the maximum value shown in Figure 1.1. As the ramp-up, snap-down motion was continued, the lift coefficient would vary, on the average, about the value at $\alpha = 20^\circ$. The value of C_L at $\alpha = 20^\circ$ is then 1.5 times C_L _{max static}. A similar approach was applied to the section drag data in order to obtain a reasonable drag penalty associated with the increased lift (i.e. the value of C_d at $\alpha = 20^\circ$). Therefore, the drag rise due to this augmented lift is

assumed to be

$$C_{d_{dyn}} = 1.1 C_{d_{max \text{ static}}} \quad (2.8)$$

Because the section moment coefficient does not change up to the $\alpha = 20^\circ$ position, a moment penalty is not imposed. Although the lift multiplier of 1.5 is considerably higher than actually achieved, Stephen's work did indicate that 1.5 might be attained. Also, if no performance benefit is seen with 1.5, then no benefit would likely exist for the type of mission investigated here.

Three variations of the baseline cruise missile were designed. These three vehicles are identical to the baseline except for their respective wing sizes. All three vehicles are capable of producing dynamic-stall-induced lift equal to the maximum usable static lift coefficient (0.8 times $C_{L_{max \text{ static}}}$) of the baseline vehicle. From Appendix A, $C_{L_{max \text{ static}}}$ for the baseline is 1.327 based on a wing reference area of 13 square feet (S). 0.8 times $C_{L_{max \text{ static}}}$ would then be 1.109. The planform area of the dynamic-lift-capable wings must be reduced to achieve a $C_{L_{max \text{ dyn}}}$ of 1.109 (where $C_{L_{max \text{ dyn}}}$ here is referenced to 13 square feet). Therefore for

the baseline vehicle

$$C_{L_{\max B}} = 0.8 C_{l_{\max}} / [1 + (m_0 / \pi AR_B)] \quad (2.9)$$

The section lift coefficient, $C_{l_{\max}}$, of a 0015 airfoil is found from extrapolated data in Abbott and von Doenhoff [23]. The maximum required lift for the design of the baseline vehicle is then

$$L_{\max \text{ design}} = 0.8 C_{l_{\max}} q S_B / [1 + (m_0 / \pi AR_B)] \quad (2.10)$$

If dynamic motion is used to achieve the maximum design lift then

$$L_{\max \text{ design}} = C_{L_{\max \text{ dyn}}} q S_{\text{dyn}} \quad (2.11)$$

Where S_{dyn} is the wing area of the new dynamic-lift capable vehicles. Since the dynamic wing is assumed to have a lift cap-

ability of 1.5 times the baseline, then

$$C_{L_{\max \text{ dyn}}} = 1.5 C_{l_{\max}} / [1 + (m_0 / \pi AR_{\text{dyn}})] \quad (2.12)$$

substituting Equation 2.12 into 2.11

$$L_{\max \text{ design}} = 1.5 C_{l_{\max}} q S_{\text{dyn}} / [1 + (m_0 / \pi AR_{\text{dyn}})] \quad (2.13)$$

Since all vehicles must achieve the same required lift, $L_{\max \text{ design}}$, Equations 2.10 and 2.13 can be combined

$$\frac{1.5 C_{l_{\max}} q S_{\text{dyn}}}{[1 + (m_0 / \pi AR_{\text{dyn}})]} = \frac{0.8 C_{l_{\max}} q S_B}{[1 + (m_0 / \pi AR_B)]} \quad (2.14a)$$

$$S_{\text{dyn}} = 0.533 S_B \frac{[1 + (m_0 / \pi AR_{\text{dyn}})]}{[1 + (m_0 / \pi AR_B)]} \quad (2.14b)$$

For $C_{l_{\max}}$ equal to 1.0 [23], a baseline wing area, S_B , of 13 square feet, and assuming the section lift-curve slope, m_0 , is 2π ,

Equation 2.14b reduces to

$$S_{dyn} = 6.0089 (1 + 2 / AR_{dyn}) \quad [ft^2] \quad (2.15)$$

Equation 2.15 is plotted in Figure 2.5. Since the wing planform is rectangular where :

$$AR = b / c \quad (2.16)$$

and

$$S = b c \quad (2.17)$$

Equation 2.15 can also be written :

$$S_{dyn} = 6.0089 (1 + 2 c_{dyn} / b_{dyn}) \quad (2.18)$$

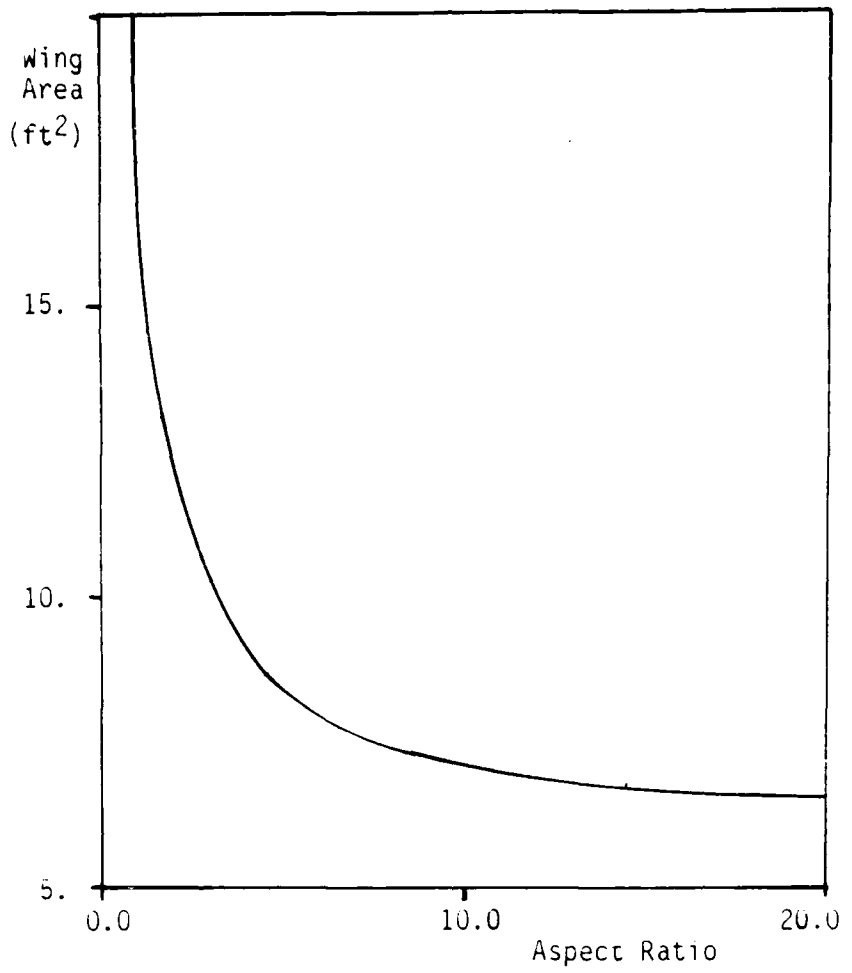


Figure 2.5. Reduced Wing Area Criteria for the Dynamic-Lift Vehicles

By fixing a value of chord, span, or aspect ratio, all geometric values of the new wing can be found using an iterative procedure with Equations 2.15 through 2.18.

The most effective means to size the smaller wing in terms of drag reduction is presented by Kohlman [24]. If the parasite drag coefficient and span efficiency factor are assumed constant, wing drag at any flight condition can be given as :

$$D_W = D_{P_R} b c / b_R c_R + (D_{W_R} - D_{P_R}) (b_R^2 / b^2) \quad (2.19)$$

where D_{P_R} is the reference wing profile drag and D_{W_R} is the total drag of the reference wing. Equation 2.19 can be normalized with respect to D_{W_R} :

$$D = D_W / D_{W_R} = P b c / b_R c_R + (1 - P) (b_R^2 / b^2) \quad (2.20)$$

where P is the ratio of parasite to total drag. If only the wing chord is reduced and the span remains constant, the change in

normalized drag can be expressed as :

$$dD = P \frac{dc}{c_R} \quad (2.21)$$

Equation 2.21 shows that there is no limit (other than structural limits) to the amount of drag reduction available due to chord reduction only. If wing span is reduced and chord is kept constant, the change in normalized drag can be expressed as :

$$dD = \left(\frac{1}{b_R} \right) [P - 2(1-P) \left(\frac{b^3}{b_R^3} \right)] db \quad (2.22)$$

If a reduction in span is to result in a net reduction of drag, dD/db must be greater than zero when $b = b_R$. This is true only if P is greater than $2/3$. Therefore, the parasite drag must be more than double the induced drag for a situation where induced drag is increasing as span is decreasing. If $P = 2/3$ and $dD/db = 0$ in Equation 2.22, a lower limit of span reduction (that gives a favorable decrease in wing drag) is established :

$$\left(\frac{b}{b_R} \right)^3 = \frac{2(1-P)}{P} \quad (2.23)$$

Equation 2.23 is plotted in Figure 2.6 [24:Fig 2].

Using Kohlman's work as a guide, three different wing sizing schemes were developed : a.) An approach where the span of the dynamic wing is keep the same as the baseline while reducing chord. This vehicle is referred to as Vehicle 3 throughout the report; b.) An intermediate approach by keeping the aspect ratio the same as the baseline while reducing both chord and span. This vehicle is referred to as Vehicle 2 throughout the report; and c.) An approach where the chord of the dynamic wing is kept the same as the baseline while reducing span. This vehicle is referred to as Vehicle 1 throughout the report. With the above criteria, the three different wings were sized and a summary of all four vehicles is presented in Table 2.1. The total-drag polars for the four vehicles are plotted in Figure 2.7 and are all referenced to the same wing area S_B (i.e. 13 square feet). Appendix A contains the equations for the three dynamic vehicle drag polars. Vehicle 1 is plotted on Figure 2.6 where it is seen to fall below the span reduction limits discussed by Kohlman. Since Vehicles 2 and 3 are also chord reduced, tney cannot be meaningfully plotted on Figure 2.6.

Design Limitations

In order to keep the vehicle design and analysis simple, several design issues were not addressed :

- 1) Structural integrity of the wing - The assumption is made that the reduced wings will withstand increased

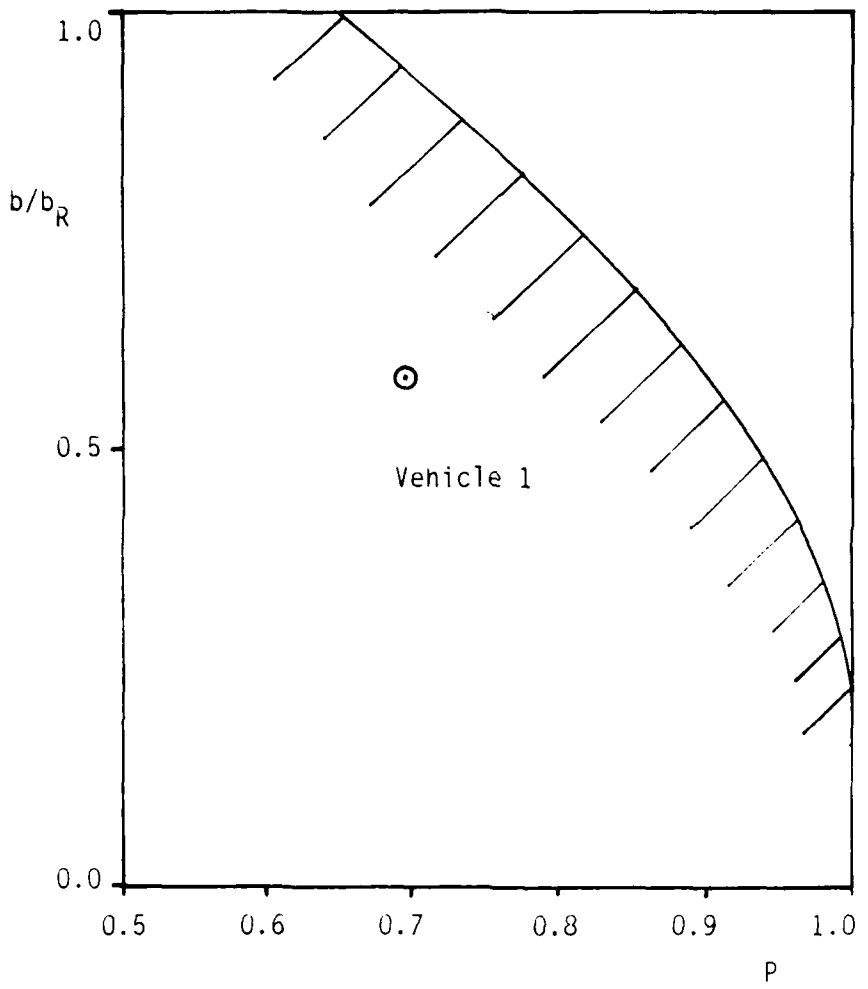


Figure 2.6. Limit of Span Reduction to Decrease Drag. From Kohlman [24:Fig 2]

Table 2.1
Comparison of Four Vehicle Configurations

	SPAN (FT)	CHORD (FT)	S (SQFT)	AR
BASELINE	13.00	1.000	13.00	13.00
VEHICLE 1	7.59	1.000	7.59	7.59
VEHICLE 2	9.49	0.730	6.93	13.00
VEHICLE 3	13.00	0.498	6.47	26.12

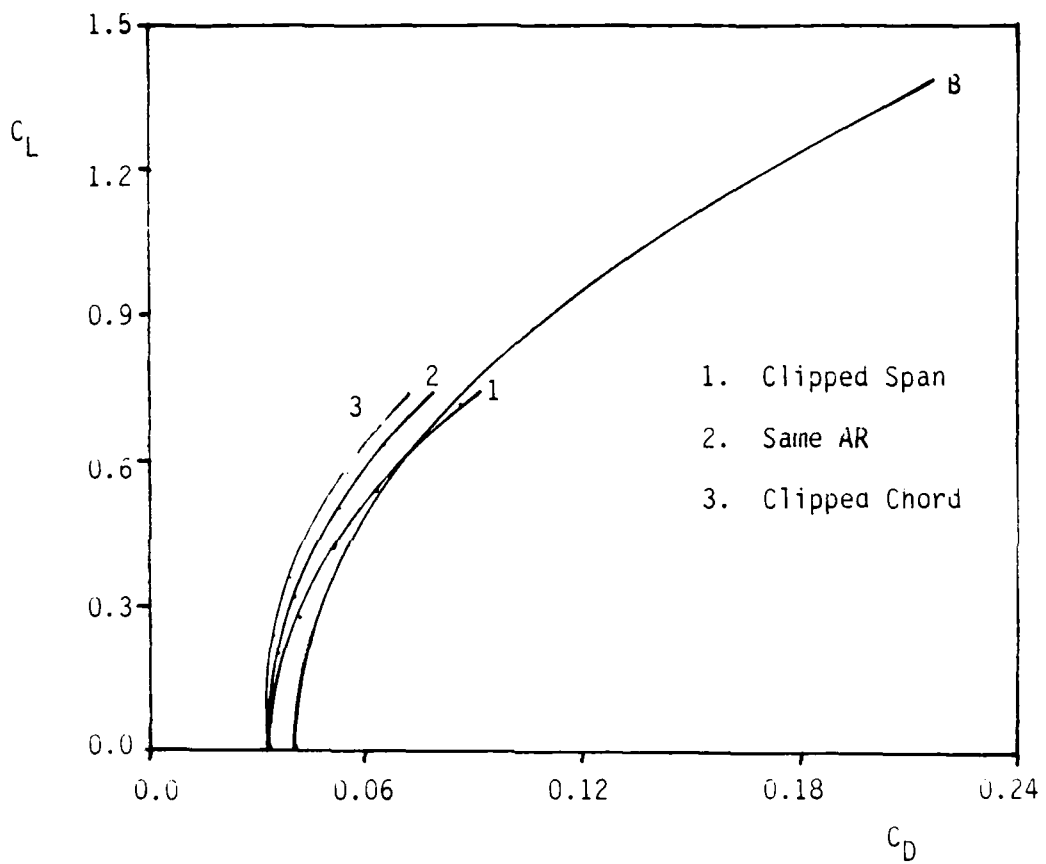


Figure 2.7. Drag Polars of Four Vehicles Based On
the Same Reference Area (13 ft^2)

wing loading, torsion, etc.

- 2) Aeroelastic effects The assumption is made that the wing is perfectly rigid.
- 3) Stability and Control The baseline vehicle and ensuing dynamic-lift vehicles were designed to be similar in size and weight to existing military hardware. Good static and dynamic stability qualities are assumed to exist.
- 4) Fuselage drag Fuselage drag is constant and not a function of angle of attack (see Appendix A).
- 5) Three-dimensional dynamic-lift effect The 3-D corrections made to the dynamic-lift wings are the same as the corrections made to the baseline vehicle.
- 6) Compressibility effects Critical mach number effects on the 0015 airfoil are not considered to effect the dynamic wings.

Structural integrity of the wing, aeroelastic effects, and stability and control, are areas that are considered beyond the scope of this investigation. Fuselage drag would only effect the baseline vehicle because the dynamic-lift vehicles are decoupled from the wing and always fly at a zero angle of attack. Three-dimensional dynamic-lift effects are not addressed because the subject has only been qualitatively addressed in the literature [25]. Compressibility effects will be addressed in Chapter 5 and Appendix B.

III. Range, Trajectory, and Mission Elements

This chapter describes the methods and equations used to compute straight-and-level operational range and longitudinal trajectory of a point mass vehicle. The computer program NSEGII [27] was used to compute the range of the four vehicles during straight-and-level cruise at sea level conditions. The computer program IIID was modified and used to predict the trajectory of the four vehicles for the following mission elements : a) CLmax climbs ; b) pull-over the top of a mountain ; and c) pull-out back to cruise altitude. Program IIID and NSEGII were both used to optimize the trajectory and range of the four vehicles over two typical terrain following missions.

Range

For an aircraft flying straight and level, the incremental distance that the vehicle can travel can be expressed as :

$$ds = V dt \quad (3.1)$$

The fuel flow or change in vehicle weight over time for a jet air-

craft can be defined as :

$$dW / dt = SFC F_N \quad (3.2)$$

where SFC is the specific fuel consumption and F_N is the net propulsive force of the vehicle. By solving Equation 3.2 for dt and substituting into Equation 3.1 :

$$ds = V dW / (SFC F_N) \quad (3.3)$$

In straight and level flight, F_N is equal to total drag force, D , and the weight, W , of the vehicle is equal to the total lift, L . If we multiply Equation 3.3 by F_N / D and L / W :

$$ds = (V dW / SFC F_N)(F_N/D)(L/W) = (V L/SFC D)(dW/W) \quad (3.4)$$

The total range is determined by integrating Equation 3.4 over the

weight change (fuel weight) of the vehicle :

$$R = \int_{W_i}^{W_f} (V L / SFC D) (dW / W) \quad (3.5)$$

If we assume that the velocity, V , remains constant throughout the flight and SFC and L/D are relatively constant for a weight change increment, then Equation 3.5 can be integrated :

$$R = (V L / SFC D) \ln (W_i / W_f) \quad (3.6)$$

Equation 3.6 is known as the Brequet range equation for a jet aircraft. NSEGII solves the Brequet equation by breaking the mission into small segments. At each segment, SFC and L/D are assumed to be constant but are updated at every consecutive segment or :

$$R = V [(L / SFC D)_1 \ln (W_i / W_2) + (L / SFC D)_2 \times \ln (W_2 / W_3) + \dots + (L / SFC D)_n \ln (W_n / W_f)] \quad (3.7)$$

Appendix C contains a sample input and output for the NNSEGII program.

Trajectory Equations

The computer program IIID [28] was used to compute the trajectory of the vehicles while traversing terrain. The program was only used in a two-dimensional mode by solving the longitudinal equations of motion for a point mass in trimmed flight, where,

$$\sum \tilde{M}_{cg} = 0 \quad (3.8)$$

$$\sum \tilde{F} = m \tilde{a} \quad (3.9)$$

Referring to Figure 3.1, Equations 3.8 and 3.9 can be written in terms of the moving vehicle reference axes (wind axes) as:

$$\sum F_x = T \cos \alpha_{BD} - D + W \sin \gamma = m \dot{V} \quad (3.10)$$

$$\sum F_z = W \cos \gamma - L - T \sin \alpha_{BD} = - m V \dot{\gamma} \quad (3.11)$$

$$\sum \tilde{M}_{cg} = 0 \quad (3.12)$$

which are the trimmed flight equations in the longitudinal plane (XZ) where γ is the flight path angle, α_{BD} is the angle of attack of the vehicle body and T is the gross thrust of the vehicle. The

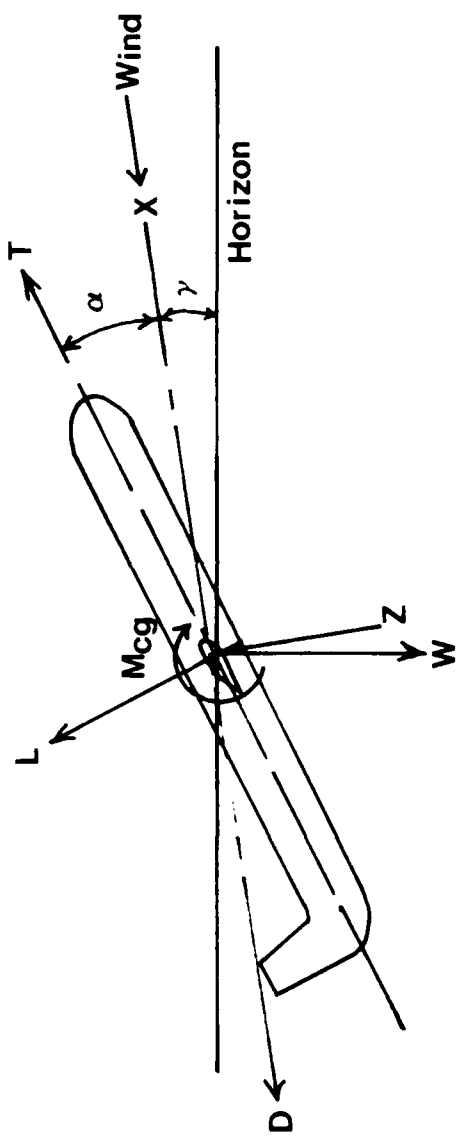


Figure 3.1. Force Diagram for a Typical Aircraft

kinematic equations which relate the moving vehicle reference axes to the earth-fixed axes (flat earth) are :

$$\dot{Y} = V \cos \gamma \quad (3.13)$$

$$\dot{H} = V \sin \gamma \quad (3.14)$$

If the longitudinal load factor is defined as :

$$n = (L + T \sin \alpha_{BD}) / W \quad (3.15)$$

Equations 3.10 and 3.11 become :

$$\dot{V} = g [(T \cos \alpha_{BD} - D) / W - \sin \gamma] \quad (3.16)$$

$$\dot{\gamma} = (g / V) (n - \cos \gamma) \quad (3.17)$$

As was mentioned in Chapter 2, the wings for the dynamic-lift vehicles are decoupled from the vehicle fuselage. Therefore, the fuselage angle of attack, α_{BD} , for these vehicles can be set at

any arbitrary α_{BD} . If α_{BD} is set at a very large angle, the thrust component in the Z direction will increase the longitudinal load factor which will increase the rate of flight path angle change. Conversely, the acceleration of the vehicle in the X direction will be decreased due to the increase in vehicle drag and decrease of the thrust component. This particular effect has not been studied in this investigation because of unknown stability and control effects that would be introduced into the problem. Therefore, for simplicity, α_{BD} is assumed to be zero in the calculation of vehicle trajectory for all of the vehicles. Although an α_{BD} of zero is physically impossible for the baseline vehicle, the understanding is that the dynamic-lift vehicles can be set at the same α_{BD} as the baseline. This particular assumption does not affect the relative performance between the four vehicles and the effect of arbitrary α_{BD} for the dynamic-lift vehicles does not enter into the problem.

Equations 3.16 and 3.17 then become :

$$\dot{V} = g [(T - D) / W - \sin\gamma] \quad (3.18)$$

$$\dot{\gamma} = (g / V) (n - \cos\gamma) \quad (3.19)$$

where,

$$n = L / W \quad (3.20)$$

Equations 3.18 and 3.19 are numerically integrated by employing the fourth-order Runge-Kutta method. Sample input and output for program IIID is found in Appendix D.

Mission Elements

The computer program IIID was used to compute the trajectory of the four vehicles for a series of cruise-missile-type vehicle maneuvers which were outlined at the beginning of the chapter. During each maneuver, the relative performance of the three dynamic-lift vehicles will be compared to the performance of the baseline vehicle. The parameters of interest for the climb, pull-over, and pull-up maneuvers are :

1. Time to final altitude
2. Minimum initial distance from terrain to begin a maneuver.
3. Maximum attainable altitude.

Time to final altitude and minimum initial distance from terrain apply to climb, pull-over, and pull-up whereas time to final

altitude only applies to the climb maneuver. All maneuvers are performed when the vehicles are at maximum lift. For the pull-over maneuver, the dynamic-lift vehicles are capable of producing the same negative lift ($C_{L_{max}} = -1.109$) as positive lift. Although cruise-missile-type vehicles also have negative lift capability, the maximum value is limited because of vehicle angle of attack limitations. The wing for the baseline vehicle shown in Figure 2.2 is fixed at some nominal angle of attack, α_0 , to produce the required lift at an average flight condition. An assumed average flight condition would be straight and level flight at half the fuel weight, or,

$$W_{avg} = L_{avg} = 1200 + (0.5)(1800) = 2100 \text{ lbs} \quad (3.21)$$

Therefore, at sea level standard conditions with a freestream Mach number of 0.5 :

$$C_{L_{avg}} = L_{avg} / (qS) = 0.4363 \quad (3.22)$$

From Equation A.13 in Appendix A :

$$C_{l_{avg}} = C_{L_{avg}} [1 + (m_0 / \pi AR)] \quad (3.23)$$

For the baseline vehicle, $C_{l_{avg}}$ is equal to 0.5034. The fixed angle of attack of the wing with respect to the vehicle body, α_0 , would then be 4.7 degrees. In order to obtain a lift coefficient value of $C_L = 1.109$ in the positive direction, the baseline vehicle must traverse to an angle of attack, α_{BD} , of 12 degrees. The assumption is then made that the vehicle cannot exceed $\alpha_{BD} = 12$ degrees in the negative direction. The relative wing angle of attack in the negative direction would then be :

$$\alpha_{wing_{neg\ max}} = \alpha_{BD_{neg\ max}} + \alpha_0 = -7.3^\circ \quad (3.24)$$

Therefore,

$$C_{L_{max\ neg}} = -0.693 \quad (3.25)$$

for the baseline vehicle. The baseline vehicle can only attain 63%

(i.e. $0.693/1.109$) of the maximum usable lift in the negative direction.

Complete Missions

Two full missions were chosen to represent typical terrains covered by a cruise-missile-type vehicle. The missions, which are designated light and rough are detailed in Figure 3.2. The vehicles covered the terrain through a series of optimum pull-up, pull-over, and pull-out maneuvers and the minimum time above sea level altitude was compared along with the total mission range. The time above sea level or minimum altitude is used as a representative measure of the susceptibility of the vehicles to any threat that may be encountered while completing the mission [31]. The vehicle trajectories were determined using the computer programs NSEGII and IID along with the information generated from the mission element section.

For the two missions, the assumption is made that when the dynamic-lift capability of the vehicles is "turned on", only one value of lift coefficient (i.e. 1.5 times $C_{L\max}$ static) can be produced by the dynamic-lift vehicles. Therefore, the dynamic-lift vehicles will have a "gap" in lift capability between the maximum lift coefficient in the static and dynamic modes. Although this assumption may appear to be a strict limitation imposed on the these vehicles, it does define a minimum capability in the use of dynamic-lift-producing wings. However, this assumption should not imply that dynamic-lift-producing wings will never be able to produce variable values of lift coefficient. Therefore, for portions of the

missions where the lift "gap" severely limits the performance of these vehicles, a measure of caution should be made when interpreting the results.

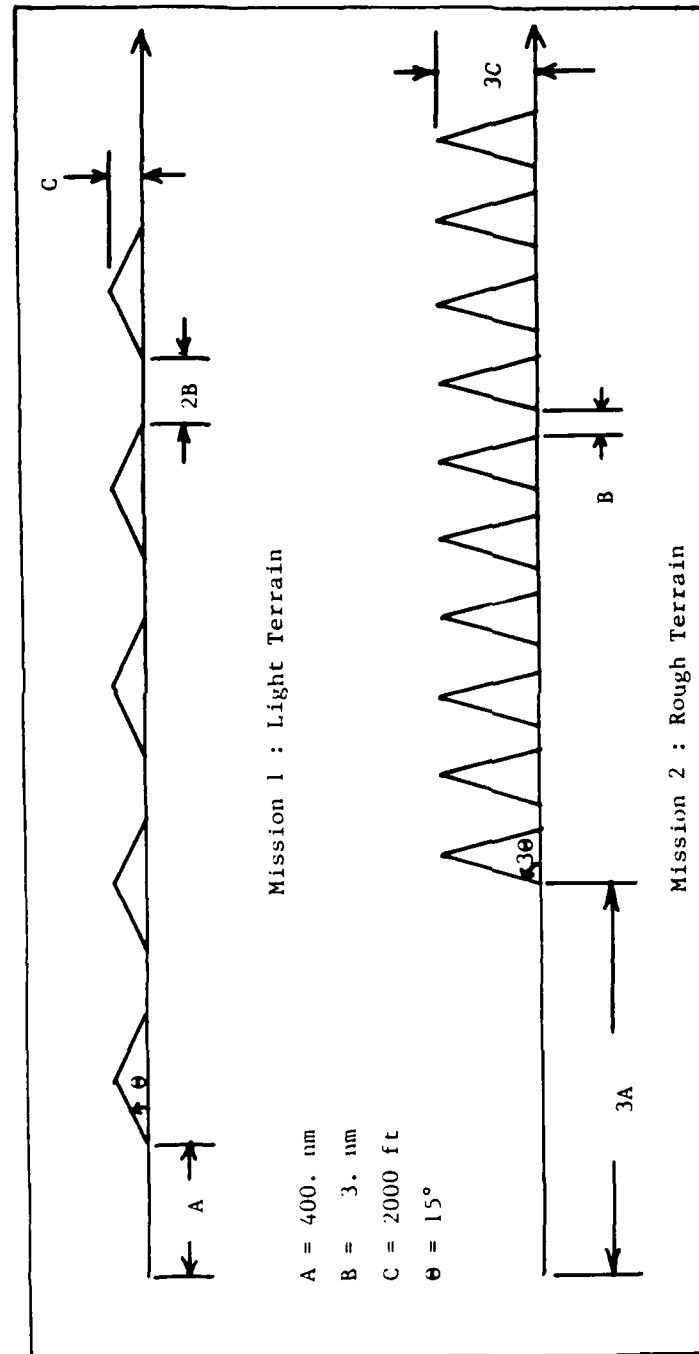


Figure 3.2. Typical Cruise-Missile-Type Missions

IV. Results and Discussion

Straight-and-Level Range

This section describes three approaches used to optimize straight-and-level range for the four vehicles discussed in Chapter 2. The resultant range of the baseline vehicle is compared to the range of the three dynamic-lift vehicles and the results are presented in Appendix D.

In the first approach, all four vehicles were flown at sea level, $M_0 = 0.5$ with the engine thrust characteristics described in Figures 2.3 and 2.4 of Chapter 2. Table D-1 of Appendix D is a summary of the results. In the second approach, the range of the four vehicles was maximized for an optimal cruise Mach number at sea level and at 10,000 feet altitude. Figures 4.1 through 4.2 and Tables D.2 through D.3 are a summary of the Mach number optimization. In the third approach, the vehicle ranges were maximized for optimal engine thrust characteristics. The engine thrust is optimized by "resizing" the engine for each of the dynamic lift vehicles. Engine "resizing" was accomplished by shifting the engine thrust curves in Figures 2.3 and 2.4 to coincide with the most efficient specific fuel consumption of the vehicle throughout the mission. As an example, the thrust vs. specific fuel consumption curve for sea level, $M_0 = 0.5$ is presented in Figure 4.3. In order to obtain the best engine efficiency for the dynamic-lift vehicles, the curve must be shifted (to the left) to the point where the bottom or bucket of the curve coincides with the nominal or average operating thrust of the vehicle.

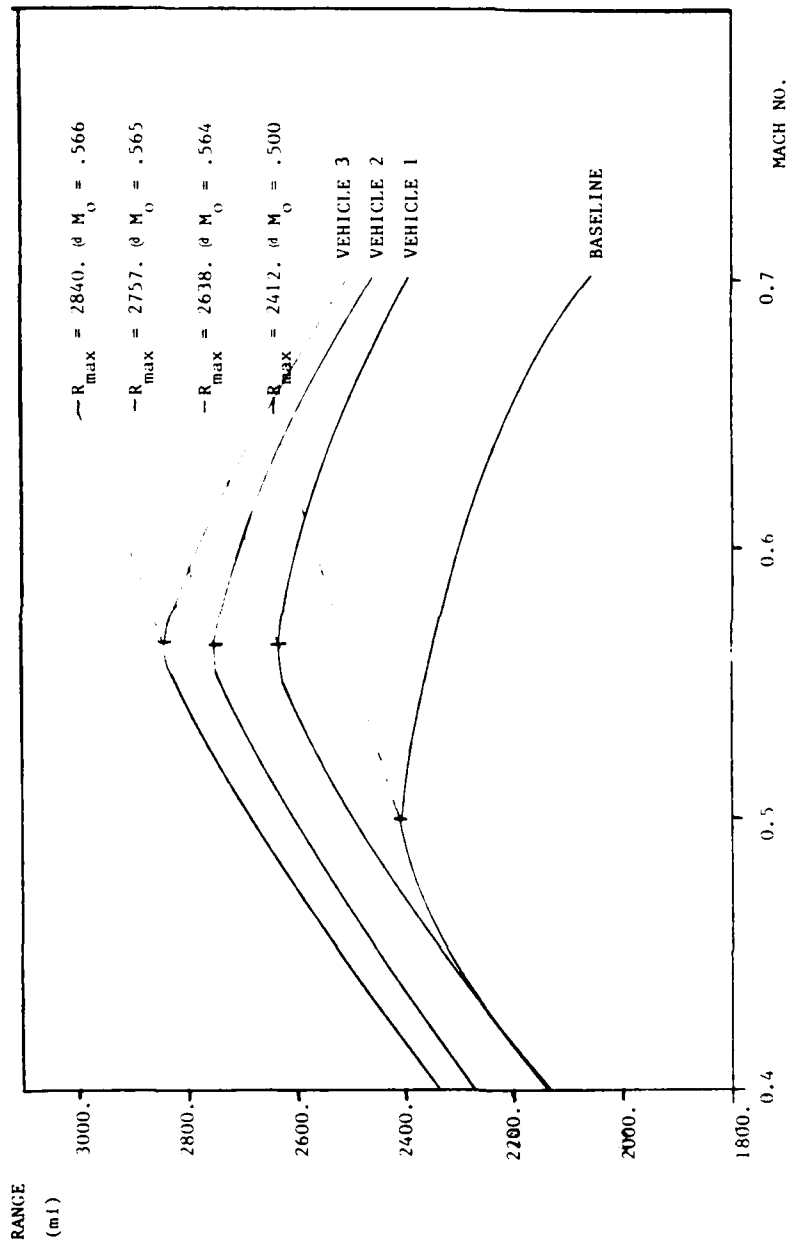


Figure 4.1. Range at Optimum Mach Number (Sea Level)

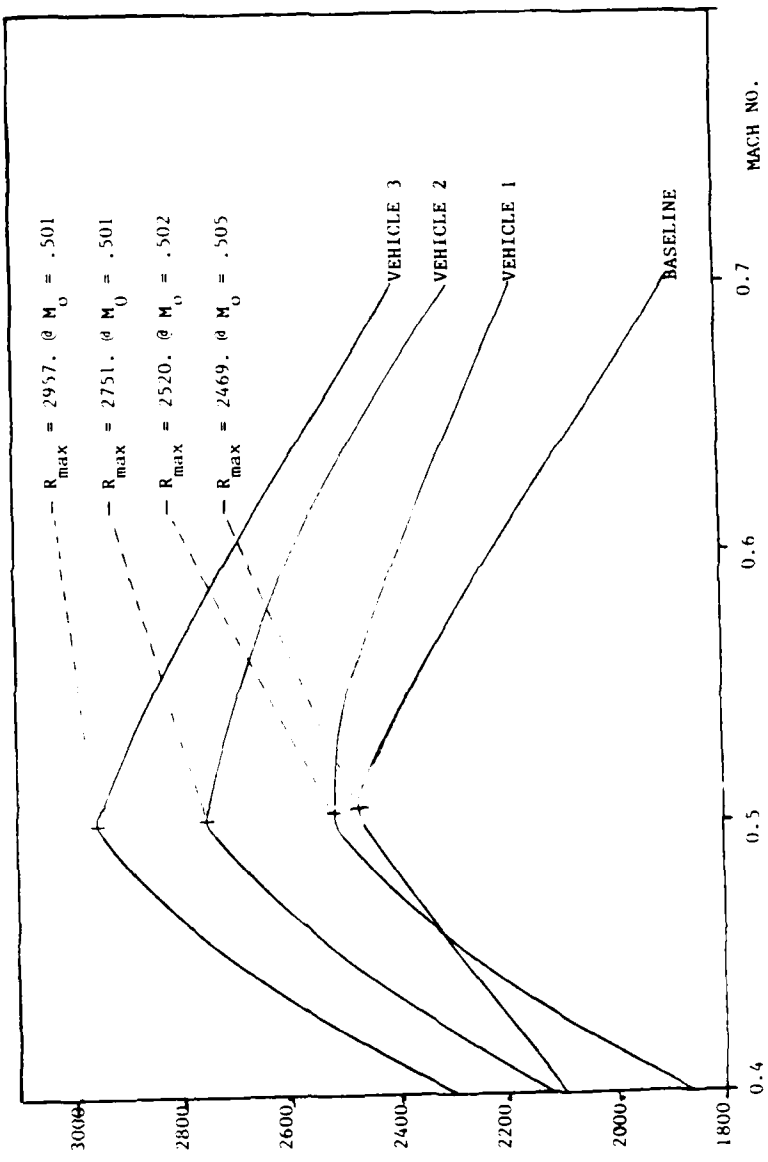


Figure 4.2. Range at Optimum Mach Number ($H = 10000$ ft)

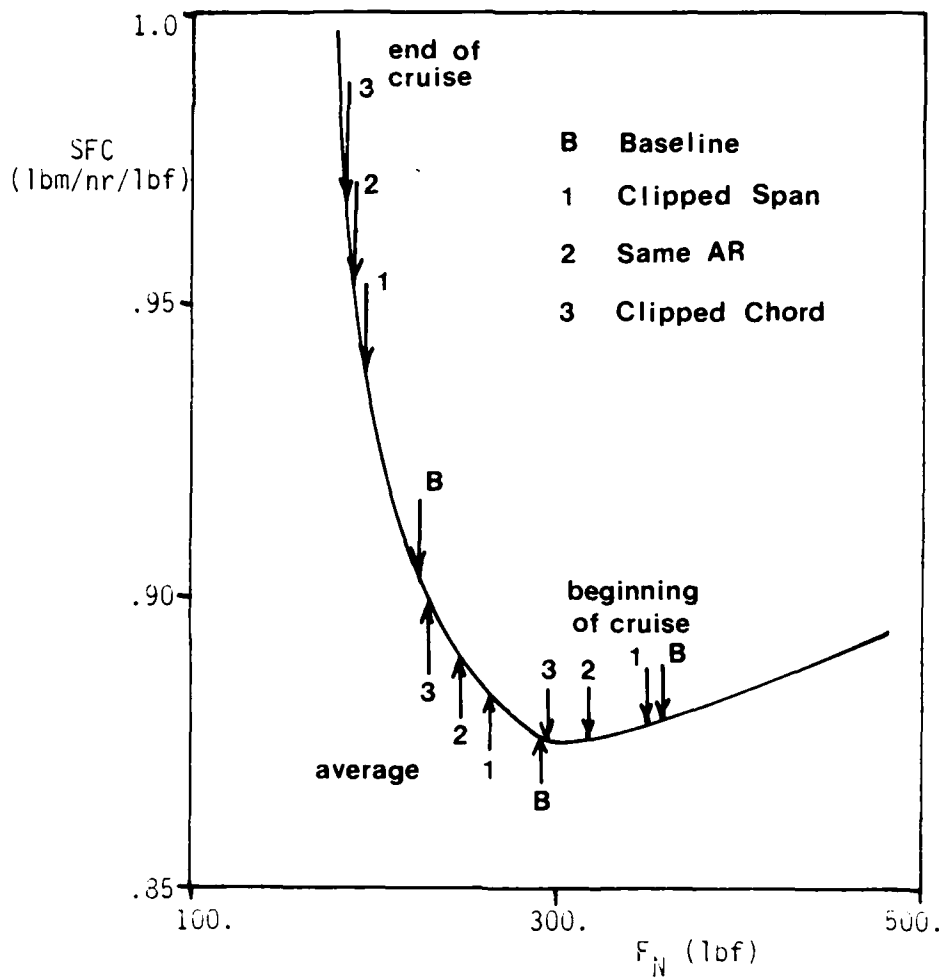


Figure 4.3. Thrust and SFC for the Four Vehicles Through a Typical Mission ($M_0 = 0.5$ at Sea Level)

Since the dynamic-lift vehicles have less drag than the baseline vehicle due to the smaller wings, they do not require as much thrust as the baseline throughout the range mission. Table D.4 is a summary of the engine thrust optimization.

A weight penalty of 100 pounds was estimated and added to the vehicle in order to account for extra weight due to the physical hardware and software that would be needed to drive the dynamic-lift wings. The penalty is imposed by reducing the fuel weight (i.e. increase the vehicle's empty weight) by 100 pounds. The effect of the weight penalty on range is also shown in Tables D.1 through D.4. The value of 100 pounds is a conservative approximation of the total weight of the equipment used in Stephen's experimental hardware. A summary of the range comparisons from Tables D.1 through D.4 is presented in Table 4.1. In all cases but one, the dynamic-lift vehicles have more range capability than the baseline vehicle. Range increases of approximately 5 to 20% occur for all three dynamic vehicles when they are engine thrust optimized while the clipped chord configuration (Vehicle 3) exhibits the best range improvements for all three optimizations. With the baseline engine, the clipped span configuration (Vehicle 1) shows a decrease in range of 2.8% when the 100 pound weight penalty is applied.

Table 4.1

Percent Change in Range With the Baseline Vehicle
For the three Optimization Techniques

	M=0.5 SL BASELINE ENGINE	MACH NUMBER OPTIMIZED	ENGINE THRUST OPTIMIZED
VEHICLE 1	+3.7 [-2.8]	+9.4 [+2.3]	+10.2 [+4.8]
VEHICLE 2	+8.2 [+1.8]	+14.3 [+7.2]	+19.3 [+13.5]
VEHICLE 3	+11.1 [+4.6]	+17.7 [+10.6]	+25.6 [+19.7]

[] = 100 LB FUEL WEIGHT PENALTY APPLIED

Mission Elements For Terrain Following

In this section, the results of the terrain following mission elements are presented and discussed. The three maneuvers are pull up to altitude, pull over terrain, and pull out of a dive to continue a sea-level-cruise mission. All maneuvers were performed at maximum thrust and maximum lift coefficient of the vehicles (maximum lift coefficient available of the baseline and maximum dynamic-lift coefficient of the dynamic-lift vehicles) and the relative performance of the three dynamic vehicles is compared to the baseline vehicle. The baseline engine was used for all four vehicles. Two of the maneuvers are performed for each vehicle at three different initial weights of 1000, 2000, and 3000 pounds to evaluate the impact of weight on performance. For the pull-over maneuver, the vehicles are evaluated at an initial weight of 2000 pounds. Although the smallest weight studied is below the minimum empty weight of the vehicle (1200 pounds) and is of little practical concern, the data for this case is useful for the development of the missions in the next section.

The first mission element to be investigated was the pull-up or climb maneuver. As a basis for comparison for the four vehicles, the maneuver was started at a Mach number of 0.5 at sea level. The ability of these vehicles to perform a $C_{L\max}$ climb are compared in Figures 4.4 through 4.5 and in Tables D.5 through D.7. In all cases, Vehicle 3 arrives at a given flight path angle and altitude faster than the other three vehicles while Vehicle 1 arrives slowest. The principal reason for the relative climb performance of the four

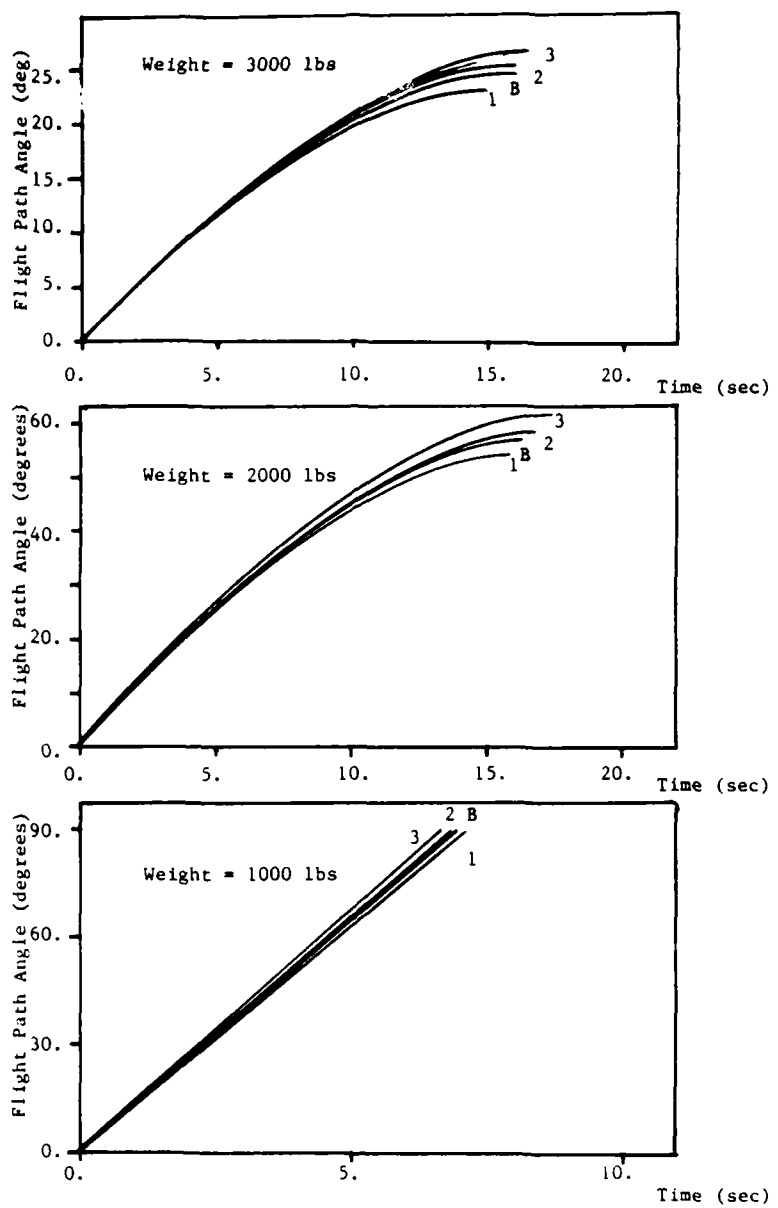


Figure 4.4. Flight Path Angle vs. Time
for a C_L_{max} Climb

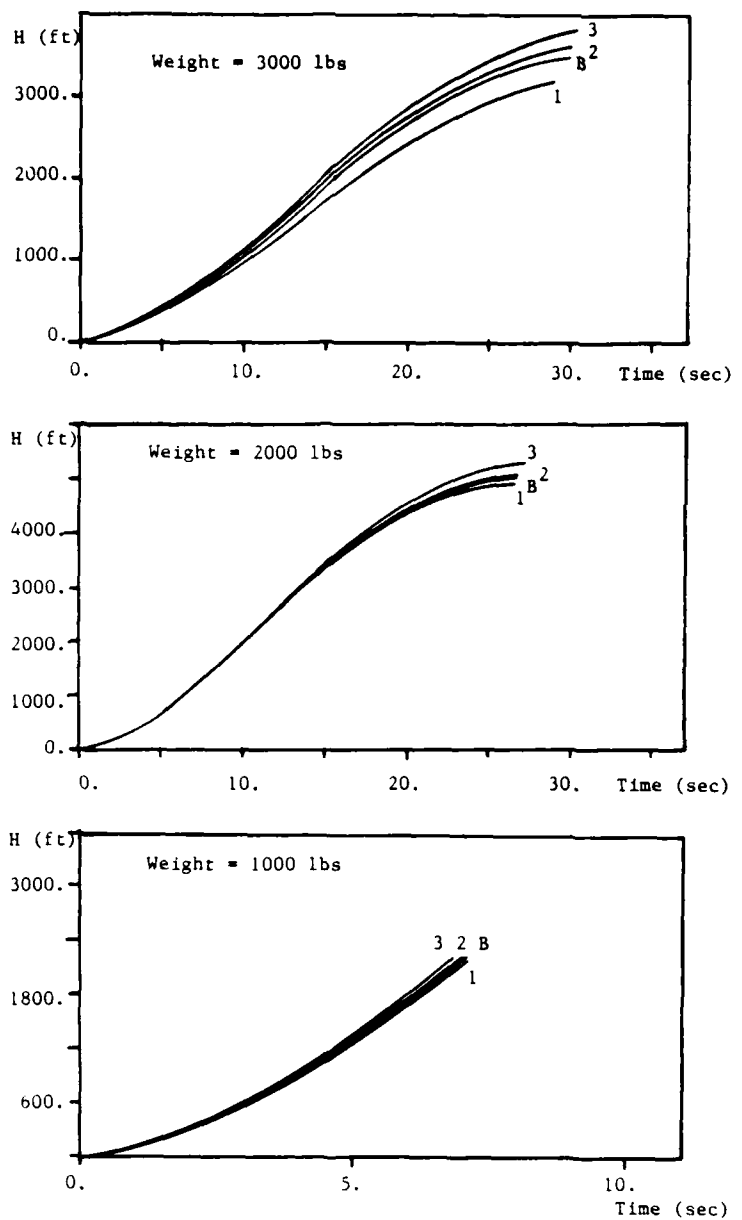


Figure 4.5. Altitude vs. Time for a

$C_{L_{\max}}$ Climb

vehicles can be attributed to the difference in drag of the four vehicles. From Figure 2.7 in Chapter 2, at $C_{L_{max}}$, Vehicle 1 has the largest drag relative to the other vehicles due to induced drag effects where vehicles 2 and 3 exhibit less overall drag. For the 1000 pound case, all four vehicles are capable of attaining a 90 degree flight path angle. Figure 4.6 contains plots of the maximum flight path angle attainable as a function of weight.

For the second element considered in terrain following, the ability of the four vehicles to pull-out from a descent was compared. The vehicles were flown at maximum thrust for four different initial flight path angles and three different initial weights. The descent was begun at an initial Mach number of 0.5. The solution was iterated to find the minimum initial altitude that the vehicle could begin the descent while reaching a final flight path angle of zero at z_e altitude. The results of the pull-out maneuvers are presented in Figures 4.7 through 4.11 and Tables D.8 through D.10.

The differences in vehicle performance are not readily apparent from the trajectory plots in Figures 4.7 through 4.11. These comparisons can be seen more vividly in Tables D.8 through D.10. The initial descent altitudes for Vehicle 2 and Vehicle 3 are less (in every case) than the altitudes for the baseline vehicle. The ability of Vehicles 2 and 3 to pull out faster is principally due to the reduced drag of these vehicles compared to the baseline. Vehicle 1, which has a higher drag coefficient than the baseline, does not perform as well as the baseline at a weight of 3000 pounds, however,

Maximum Flight Path
Angle Reached (degrees)

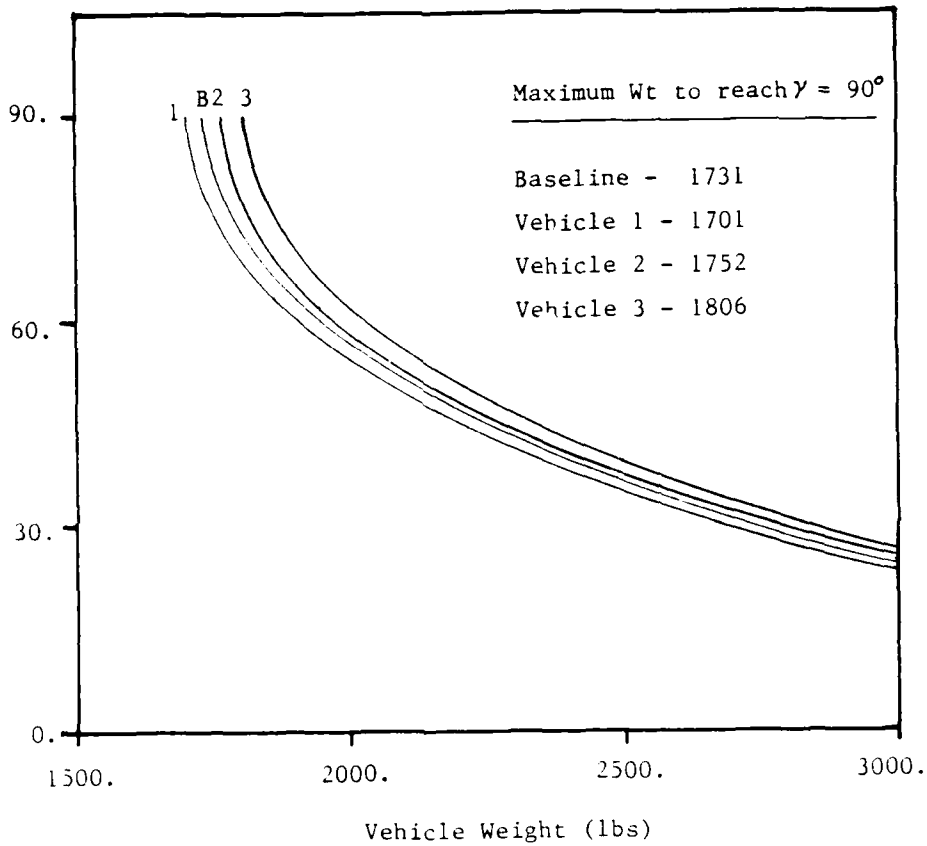


Figure 4.6. Vehicle weight vs. Achievable Flight Path Angle

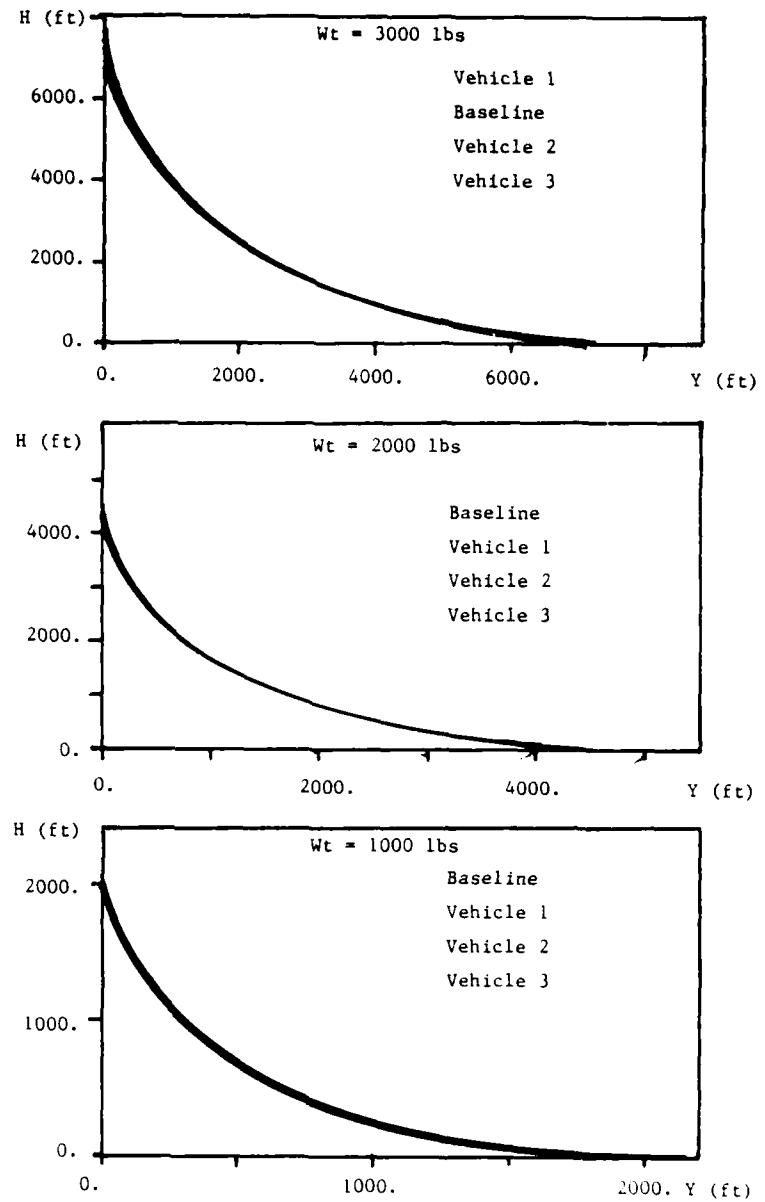


Figure 4.7. Altitude vs. Downrange
for a Pull Out From $\gamma = -90^\circ$ at Max
Thrust

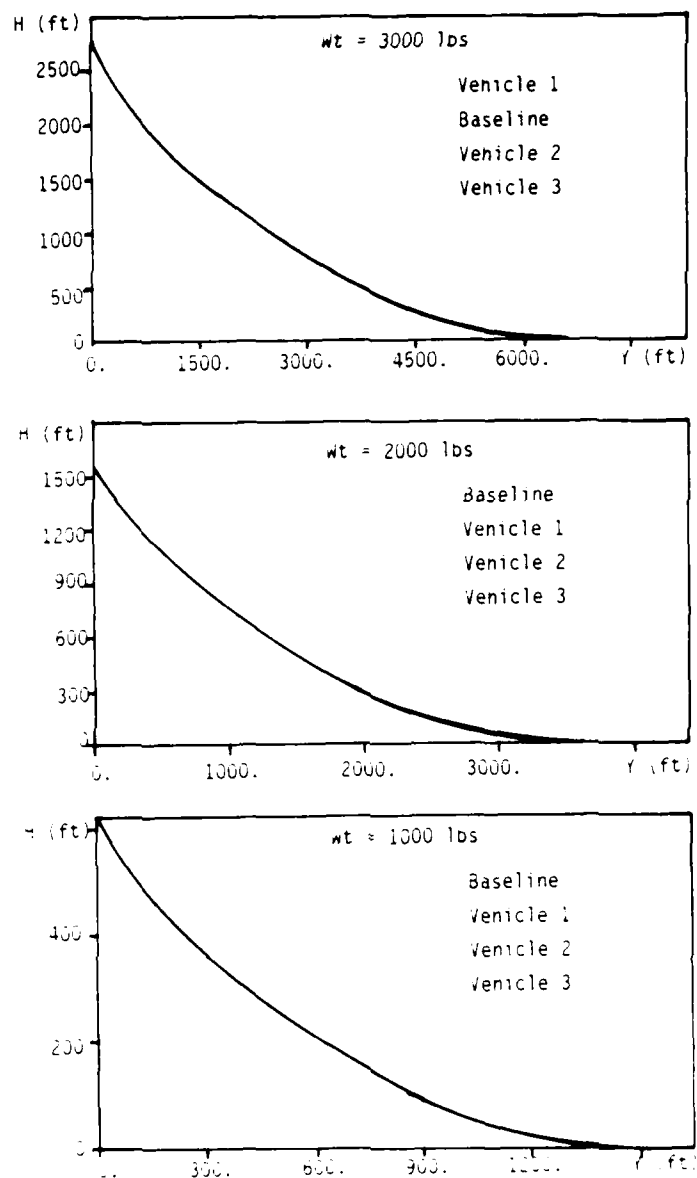


Figure 4.8. Altitude vs. Downrange
for a Pull Out from $\gamma = -45^\circ$ at Max
Thrust

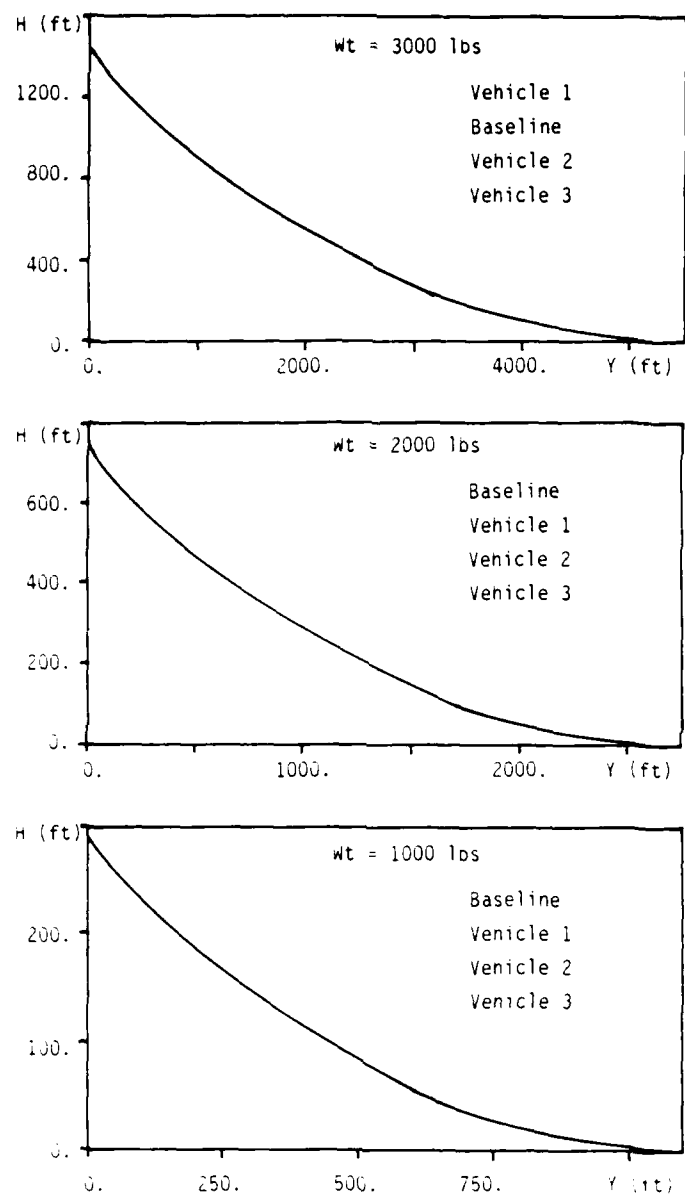


Figure 4.9. Altitude vs. Downrange
for a Pull Out from $\gamma = -30^\circ$ at Max
Thrust

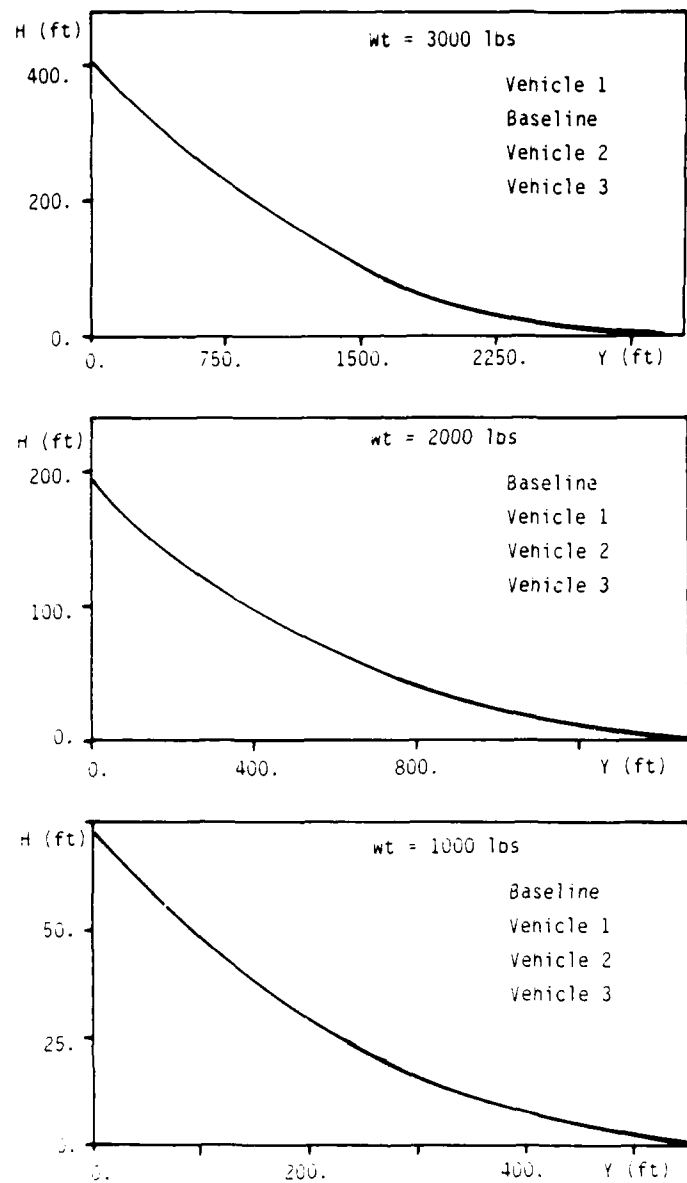


Figure 4.10. Altitude vs. Downrange
for a Pull Out from $\gamma = -15^\circ$ at Max
Thrust

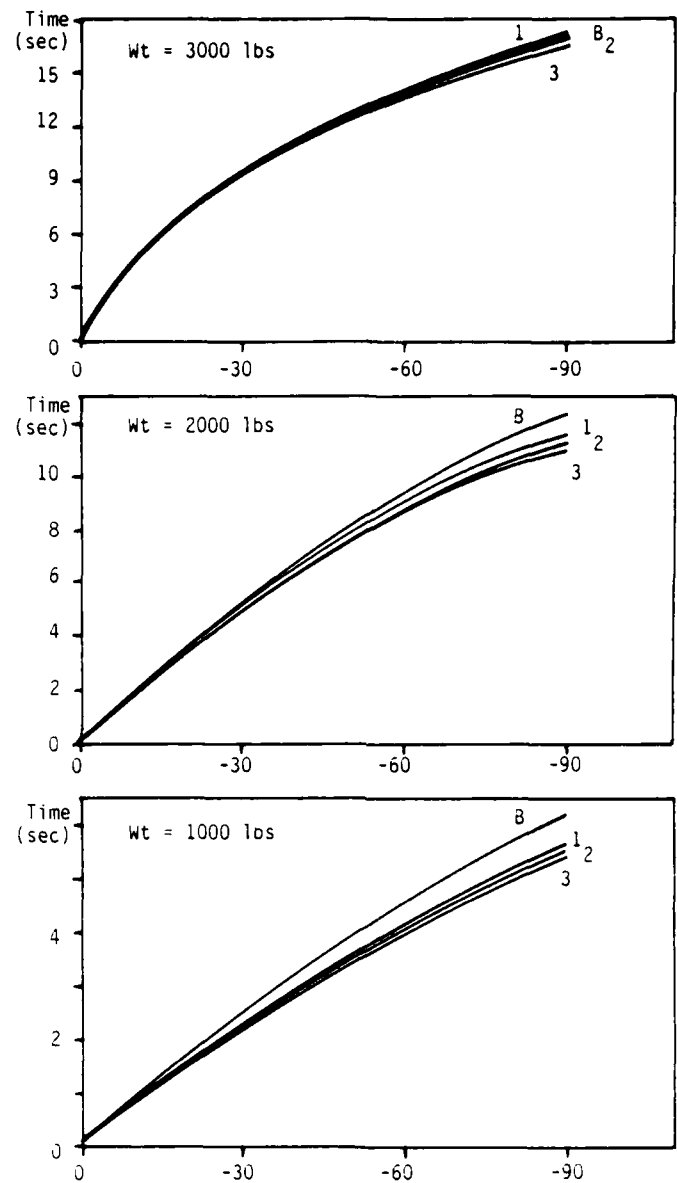


Figure 4.11. Time to Pull Out vs.
Initial Flight Path Angle at
Max Thrust

at the 2000 and 1000 pound weights, Vehicle 3 pulls out faster than the baseline. From Equations 3.18 and 3.19 of Chapter 3, it can be seen that drag is not the only factor influencing the trajectory of the vehicles. As a vehicle begins a descent, increased drag can help the maneuver by reducing altitude descent rate as the flight path angle is changing. However, at the end of the maneuver, the increased drag can impede the efficiency of the vehicle's descent to the final altitude. Therefore, the total efficiency of the maneuver is a function of thrust, weight, initial velocity, and the relative effect of drag at all portions of the maneuver. Table D.11 is an example of the effect of thrust on the minimum initial altitude for an initial velocity of zero. Although constant thrust throughout the maneuver may not be the most efficient means of pulling out, the maximum thrust criteria has been chosen in this situation to be consistent with that used for the the other mission elements. Further, it is believed that the differences shown in vehicle pull-out performance for this particular mission element are relatively small so that any attempts to improve pull-out efficiency will not greatly effect the final comparison.

The final mission element to be investigated was the pull-over maneuver. This particular element not only was difficult to analyze but showed some unusual results. Instead of presenting results similar to the first two mission elements, the focus will be on the discussion of the vehicles at one particular weight and initial flight path angle. Figure 4.12 shows the relative pull-over capability of the three dynamic vehicles compared to the baseline.

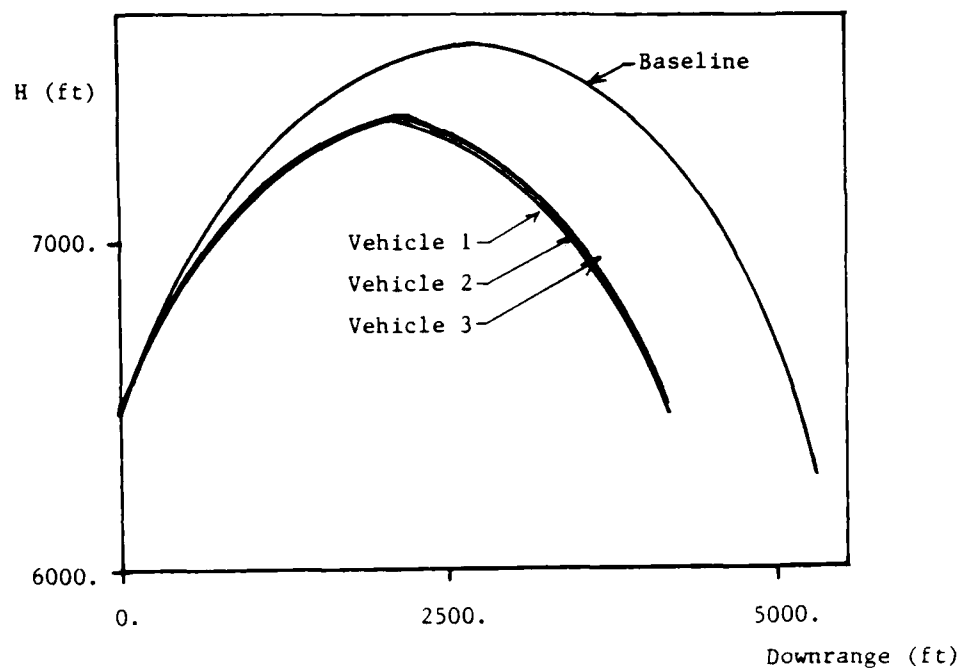


Figure 4.12. Pull-Over Maneuver from $\gamma = +45^\circ$ to -45° . Weight = 2000 lbs

From this figure it can be seen that the dynamic vehicles can pull over much sooner than the baseline. What is not evident from this figure is the behavior of the dynamic vehicles after the pull-over segment is completed. During the mission optimizations, which will be discussed in greater detail in the next section, the vehicles had difficulty recovering from this maneuver. The resultant decelerations from a negative-dynamic-maximum lift coefficient made it difficult for these vehicles to pull-out to a particular flight path angle until the vehicle had gained enough velocity to generate enough lift for the pull-out. To try and understand why these vehicles react in such a manner, the deceleration behavior of the four vehicles is shown in Figure 4.13 where P_s is defined as :

$$P_s = V (T - D) / W \quad (4.1)$$

The common name usually associated with P_s is specific excess power. At the onset of the dynamic maneuver, the dynamic vehicles experience P_s values as large as three to nine times greater than the baseline vehicle. Also, the baseline vehicle recovers from this situation quite quickly. The three dynamic vehicles, on the other hand, continue to experience the negative P_s condition for an extended period of time. There are two reasons why P_s stays negative longer for the dynamic lift vehicles. The most obvious reason is the extremely large increase in drag due to the negative-

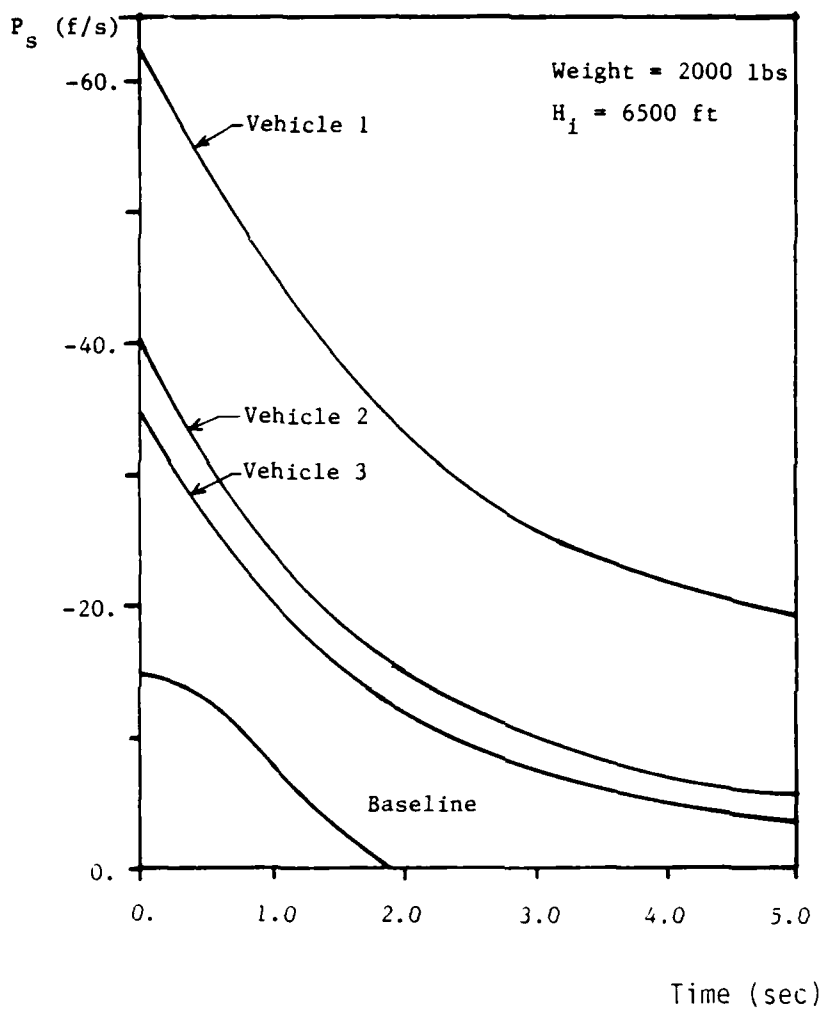


Figure 4.13. Specific Excess Power vs.
Time for the Pull-Over Maneuver in
Figure 4.12

dynamic lift. The other effect, not so readily apparent is the reduction in maximum thrust due to increased altitude and decreased Mach number (see Figures 2.3 and 2.4). The result is extremely rapid decelerations. The dynamic vehicles do reach the desired negative flight path angles quickly as shown in Figure 4.12, but when positive lift is applied, the dynamic vehicles continue to descend into a steeper dive until enough vehicle velocity is attained to pull out. The results of this effect are shown clearly in mission number one in the next section.

Missions

Two full missions were developed for this investigation in order to compare the terrain following capability of the dynamic-lift vehicles to the baseline vehicle. The baseline engine is used for all four vehicles and all terrain following maneuvers are performed at maximum thrust. The measures of merit for the comparison of the four vehicles is : a) the total amount of time that the vehicle is above the minimum sea level altitude ; and b) the total mission range of the vehicles. The range calculation was performed by breaking each mission into three segments and computing the fuel loss for : a) the straight and level portion of the flight at the beginning and end of the mission ; b) the portion of the flight when the vehicle traverses the mountains ; and c) the segment of straight-and-level flight between the mountains. In order to compute the fuel loss for the first and third segment, Figure 4.14 was constructed from the NNSEGII calculation of straight-and-

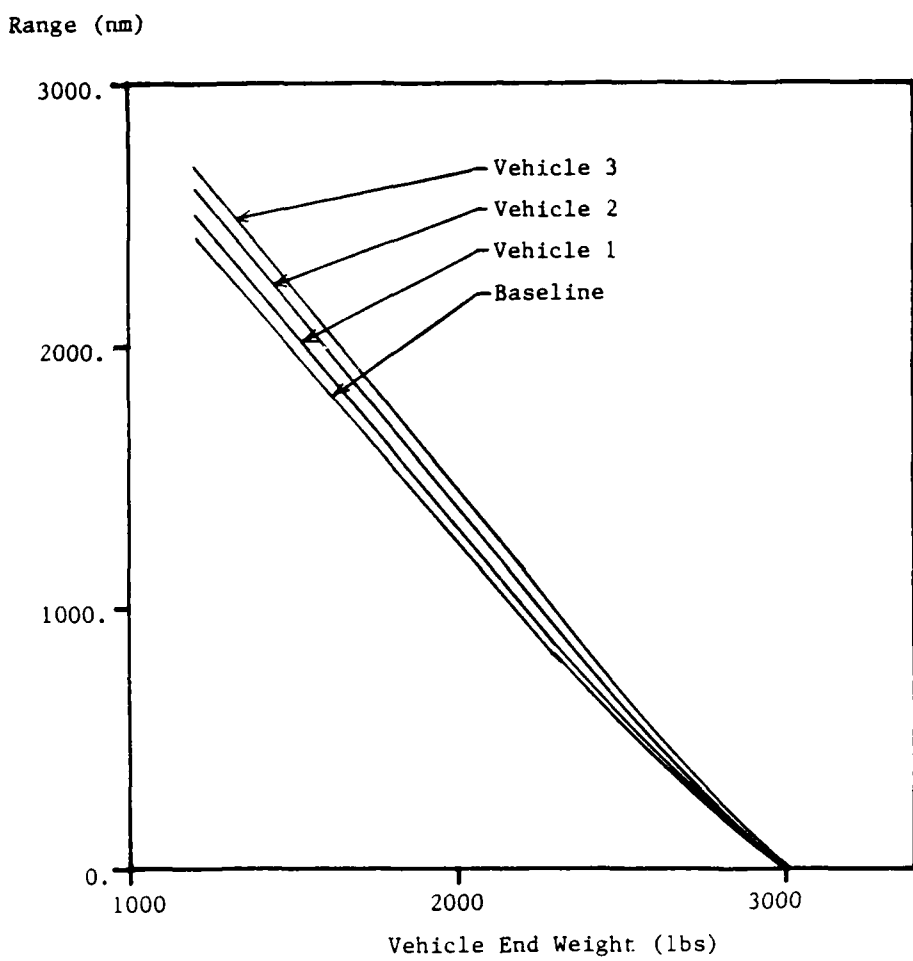


Figure 4.14. Vehicle Weight vs. Range for
Mission Planning

level range and used to compute fuel loss for the pre-terrain, between terrain, and post-terrain portions of the mission. Figure 4.15 was constructed by computing an average fuel loss at maximum thrust for each of the four vehicles and is used to compute the fuel loss of the vehicles during the terrain following portion of the mission. The distance covered in Figure 4.15 is the total distance that each vehicle traverses traveling up and over each mountain. The trajectory and time above minimum altitude during the terrain following portion is computed for one mountain and then multiplied by the total number of mountains in the mission.

For Mission 1, the four vehicles were flown straight and level for 400 nautical miles until the terrain was reached. Figure 4.16 is a depiction of the trajectories optimized for this mission; Tables D.12 through D.15 are a summary of the various mission elements required to perform an optimal trajectory over each mountain; Table D.16 shows the fuel loss estimates for the terrain following portions of the mission; and Table 4.2 is a summary of the total mission range and time above sea level for each vehicle.

The baseline vehicle is able to pull up and over the terrain by following the contour of the mountain. However, the dynamic vehicles are forced to use their dynamic-lift capability for the entire climb phase of the mission in order to get over the terrain. Because the assumption was made that the dynamic-lift vehicles are only capable of attaining one value of dynamic-lift, these vehicles are not able to climb at a constant flight path angle along the mountain contours before the static-maximum-lift coefficient and peak altitude is

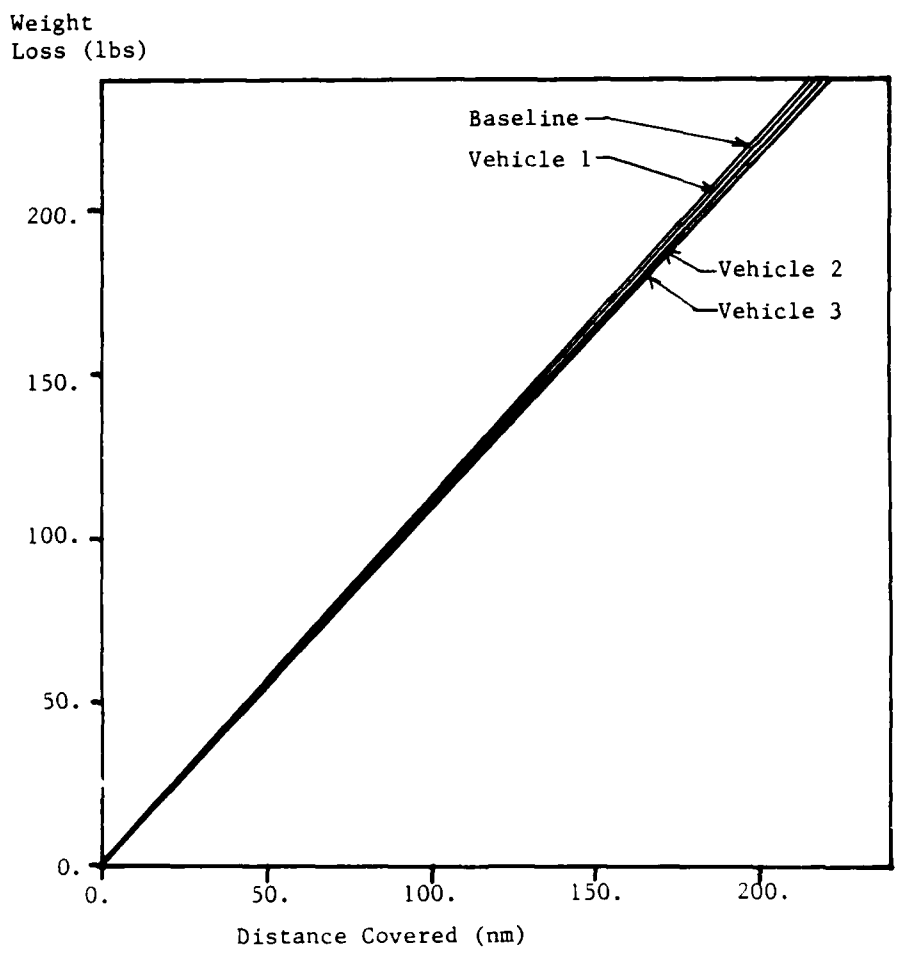


Figure 4.15. Average Weight Loss vs. Distance Covered During the Terrain Following Mode

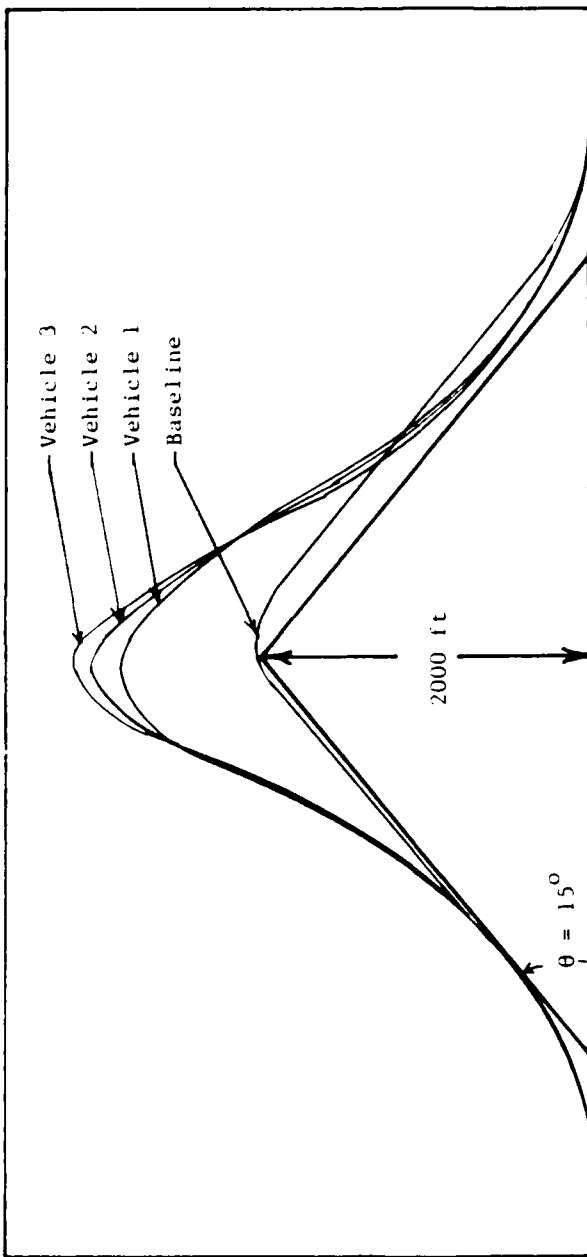


Figure 4.16. Vehicle Trajectories for Mission 1

Table 4.2

Mission 1 - Range and Time Above Sea level
For All Four Vehicles

	PRE-TER. MILES (NM)	TERRAIN HORIZONTAL MILES(NM)	TOTAL MISSION RANGE(NM)	% INCREASE OVER BASELINE	TOTAL TIME ABOVE SEA LEVEL(SEC)
BASE	400.0	36.72	2399.2	-----	183.4
VEH. 1	400.0	36.72	2494.2 [2344.1]	+3.96 [-2.29]	238.4
VEH. 2	400.0	36.72	2574.2 [2396.7]	+7.29 [-0.10]	237.85
VEH. 3	400.0	36.72	2659.2 [2506.7]	+10.84 [+4.48]	237.65

[] = 100 LB FUEL WEIGHT PENALTY APPLIED

reached. Therefore the dynamic vehicles must perform a dynamic C_L max climb to a point near the maximum attainable flight path angle and then essentially "fall" back to the sea level altitude. Although the trajectory overshoot is minimized by making use of the negative lift capability of these vehicles, this particular mission indicates some of the difficulties encountered when the dynamic vehicles are limited to only a single value of augmented lift.

From Table 4.2, It is apparent that total mission range along with the total time above minimum altitude for the dynamic vehicles is adversely affected by the extra distance that must be travel due to the "gap" in static and dynamic lift. This mission clearly shows that a variable dynamic-lift capability is necessary in order to gain an advantage over the baseline vehicle in a conventional terrain following mode.

In Mission 2, where the terrain following requirements are more severe than Mission 1, the baseline vehicle is forced to utilize the maximum lift in order to clear the terrain. Figure 4.17 is a depiction of the vehicle trajectories optimized for this mission; Tables D.17 through D.20 are the mission elements necessary to optimize the trajectories; Table D.21 is a summary of fuel loss estimates for the terrain following portion of the mission; and Table 4.3 is a summary of the total mission range and total time above sea level for the complete mission.

In order to attain enough altitude to clear the terrain, all four vehicles were optimized to perform the maximum constant g climb that would allow them to gain enough altitude to clear the 5000 ft.

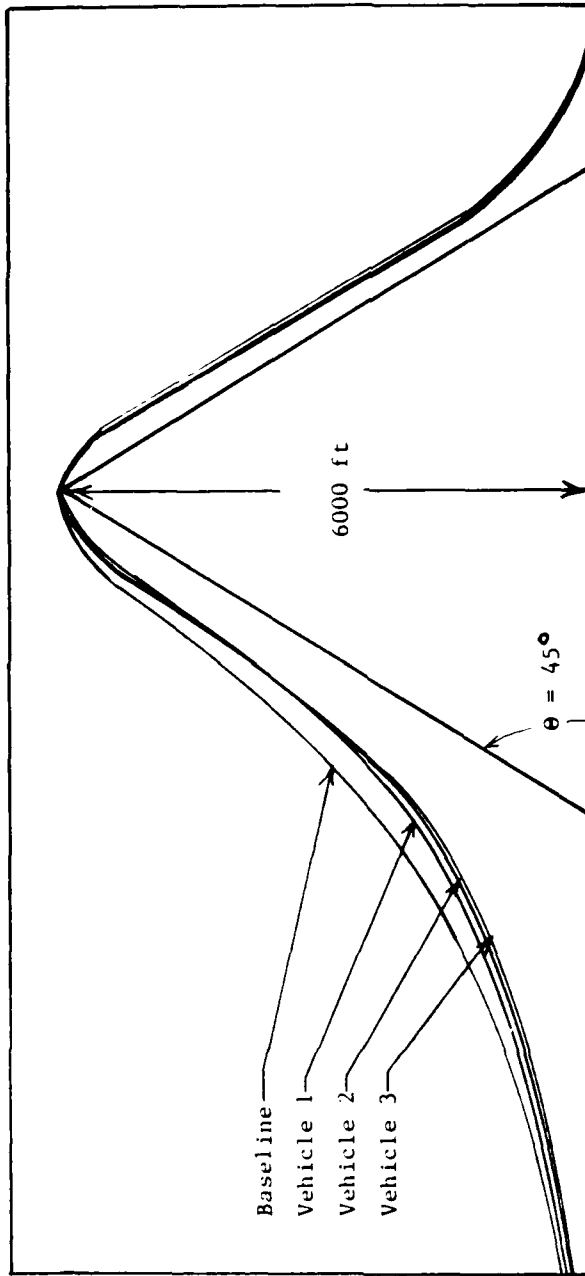


Figure 4.17. Vehicle Trajectories for Mission 2

Table 4.3
Mission 2 - Range and Time Above Sea Level
For All Four Vehicles

	PRE-TER. MILES (NM)	TERRAIN HORIZONTAL MILES(NM)	TOTAL MISSION RANGE(NM)	% INCREASE OVER BASELINE	TOTAL TIME ABOVE SEA LEVEL(SEC)
BASE	1200.0	46.75	2314.3	-----	681.20
VEH. 1	1200.0	46.75	2386.7 [2236.3]	+3.13 [-3.35]	701.20
VEH. 2	1200.0	46.75	2491.8 [2319.3]	+7.67 [+0.21]	664.60
VEH. 3	1200.0	46.75	2574.3 [2431.8]	+11.23 [+5.07]	646.00

[] = 100 LB FUEL WEIGHT PENALTY APPLIED

mountains. When static-maximum lift coefficient was reached for the dynamic vehicles, the dynamic-lift capability was used to reach the peak altitude. All vehicles used a similar approach to pull over and out of the terrain. In this case, Vehicles 2 and 3 have a clear advantage when performing a maneuver similar to the baseline because they have less drag than the baseline. With the optimized combination of a constant g climb and a constant dynamic climb and descent, Vehicles 2 and 3 can travel up and over the terrain faster than the baseline. Vehicle 1 cannot perform the maneuvers as quickly as the baseline because of the relatively high induced drag produced by the low aspect ratio wing.

In both missions, the three dynamic vehicles maintain a range advantage over the baseline except when the 100 lb weight penalty is imposed. With the weight penalty, only Vehicle 3 maintains a range advantage in Mission 1, while both vehicles 2 and 3 fly farther in Mission 2. The ability of vehicles 2 and 3 to use less fuel in the pre-terrain segment of each mission works as a disadvantage to both. As all four vehicles approach the terrain following segment of the mission, vehicles 2 and 3 are heavier than the baseline. Therefore they must maneuver at a higher and more restricting weight than the baseline. It is important to indicate that these missions only show how one might optimize missions for the dynamic-lift advantage. A further improvement to these optimizations might include the consideration of the increased stand-off range that could be gained by the dynamic-vehicles if they were allowed to burn down to the same weight as the baseline vehicle. At lower weight in the terrain

following segments of the mission, the dynamic-lift vehicles would then exhibit even greater terrain following capabilities.

V. Conclusions and Recommendations

The results of this study have shown that the use of dynamic-stall induced lift augmentation can greatly improve the range and maneuver capability of a cruise-missile-type vehicle. However, due to the severe restrictions imposed on that lift capability (i.e. the static to dynamic lift "gap"), the results of two terrain following missions have shown that the dynamic-lift vehicles were only capable of out-performing the baseline vehicle in situations where the baseline was forced to use a maximum capability. Although this restriction may be considered to be too severe of a requirement, it does indicate that a variable-maximum-dynamic lift capability is necessary and should be pursued in future research in order to achieve the maximum applied benefit of the dynamic-stall event.

Of the three dynamic-lift vehicles used for this study, Vehicle 3, the clipped or reduced chord vehicle, consistently out-performed all vehicles in range and maneuver capability, whereas, Vehicle 1, the clipped or reduced span vehicle, consistently under-performed all vehicles except in some examples of pull-out to level flight.

In this study, the primary performance advantages gained by the use of dynamic-lift were mainly due to an ability to reduce wing area thereby reducing vehicle drag. Another important maneuver capability which must also be investigated is the ability of these vehicles to take advantage of an inherent thrust-vectoring capability unique to a decoupled wing-body system. A combination of thrust-vectoring and drag reduction could produce unprecedented

increases in maneuverability and performance.

Because of the potential advantages to be gained by the application of dynamic-stall induced lift several key areas should be investigated :

1. Compressibility effects on the dynamic-stall event - For this study, critical Mach number on the 0015 airfoil is achieved well before $M = 0.5$. (see Appendix B). In order to make use of the dynamic-stall event at realistic flight conditions, the effects of compressibility must be thoroughly investigated.
2. The effect of dynamic-stall producing wing motions on material stresses and aeroelastic effects.
3. Improved computer simulation models to investigate the potential performance advantages of dynamic-lift vehicles.
4. Stability and control related considerations for a decoupled wing-body system.
5. Optimizations of stand-off distance for missions where the end or termination point is fixed.

Bibliography

1. Kramer, Von M., "Die Zunahme des Maximamauftriebes von Tragflugeln bei plötzlicher Anstellwinkel-vergro Berung (Boenefekt)," Zeitschrift fur Flugtechnik und Motorluftschiffahrt, 7, 14 april 1932, pp. 185-189.
2. Carta, F. O., "Unsteady Normal Force on an Airfoil in a Periodically Stalled Inlet," J. of Aircraft, September -October 1967, pp. 416-421.
3. Ham, N. D., "Aerodynamic Loading on a Two Dimensional Airfoil During Dynamic Stall," AIAA Journal, Volume 6, No. 10, October 1968, pp. 1927-1934.
4. Deekens, A. C., and Keubler, W. R., "A Smoke Tunnel Investigation of Dynamic Separation," Aerodynamic Digest, Fall 1978, USAFA TR-79-1, Air Force Academy, February 1979.
5. Daley, D. C., "Experimental Investigation of Dynamic Stall," Master's Thesis, AFIT/GAE/AA/82D-6.
6. Dimmick, R. L., "Pitch Location Effects on Dynamic Stall," Master's Thesis AFIT/GEA/AA/85D-4.
7. Lawrence, J. S., "Investigation of Effects Contributing to Dynamic Stall Using a Momentum Integral Method," Master's Thesis, AFIT/GAE/AA/83D-12.
8. Tupper, K. W., "The Effect of Trailing Vortexes on the Production of Lift of an Airfoil Undergoing a Constant Rate of Change of Angle of Attack," Master's Thesis, AFIT/GAE/AA/83D-26.
9. Allaire, A. J. S., "Investigation of Potential Viscous Flow Effects Contributing to Dynamic Stall," Master's Thesis, AFIT/GAE/AA/84S-1.
10. Schreck, S. J., "Continued Experimental Investigation of Dynamic Stall," Master's Thesis, AFIT/GAE/AA/83D-21.
11. Daley, D. C., and Jumper, E. J., "Experimental Investigation of Dynamic Stall," J. of Aircraft, 21, September 1984.
12. Jumper, E. J., Schreck, S. J., and Dimmick, R. L., "Lift-Curve Characteristics for an Airfoil Pitching at Constant Rate," AIAA Paper Number AIAA-86-0117.

13. McAlister, K. W., Carr, L. W., and McCroskey, W. J., Dynamic Stall Experiments on the NACA 0012 Airfoil, NASA Technical Paper 1100, January 1978.
14. Stephen, E. J., "Investigation of Periodic Pitching Through The Static Stall Angle of Attack," Master's Thesis AFIT/GAE/AA/87M-4.
15. Chow, C. W., and Chiu, C. S., "Unsteady Loading on Airfoil Due to Vortices Released Intermittently from the Surface," J. of Aircraft, Volume 23, No. 10, pp. 750-755.
16. Ashley, H., "Fighter Maneuvers to Extreme Angles of Attack", Dept. of Aeronautics and Astronautics, Stanford Univ., Stanford, CA.
17. Hamilton, W. L., and Skow, A. M., Operational Utility Survey: Supermaneuverability, Air Force Wright Aeronautical Laboratories, WPAFB, OH, AFWAL-TR-85-3020, September 1984.
18. Lang, J. D., and Francis, M. S., "Unsteady Aerodynamics and Dynamic Aircraft Maneuverability," AGARD Symposium on Unsteady Aerodynamics, Goettingen, FRG, May 1985.
19. Jumper, E. J., Hitchcock, J. E., Lawrence, T. S., and Docken, R. G., "Investigation of Dynamic Stall Using a Modified Momentum Integral Method," AIAA-87-0431.
20. Nicolai, L. M., Fundamentals of Aircraft Design, METS, Inc. 1975, revision 1984.
21. Nicolai, L. M., and Pinson, J., Aircraft Design Short Course, class handout notes, Bergamo Conference, Dayton, OH, July 13-17, 1987.
22. Williams, J. C., "Incompressible Boundary-Layer Separation," Annual Review of Fluid Mechanics, 9: pp. 113-144, 1977.
23. Abbott, I. H., Von Doenhoff, A.E., Theory of Wing Sections Dover Publications Inc., 1959.
24. Kohlman, D. L., "Drag Reduction Through Higher Wing Loading," Aeronautics Digest, Air Force Academy, USAFA-TR-78-6 Spring, 1978.
25. Saharon, D., and Luttges, M., "Three-Dimensional Flow Produced By A Pitching-Plunging Model Dragonfly Wing", AIAA Paper Number AIAA-87-0121, January 1987.
26. Hoerner, S. F., Fluid-Dynamic Drag, Published by Author, P.O. Box 342, Brick Town, NJ 08723. 1965.

27. Fellows, M. S., "NSEG -- Segmented Mission Analysis Program ASD/ENFTA Users Manual," ASD/ENFTA, WPAFB, OH, ENFTA-TM-84-01, March 1984.
28. Jonas, F. M., "Three-Dimensional Maneuverability Program," Internal Document, ASD/ENFTA, WPAFB, OH, RD19T-1.
29. Kuethe, A. M., and Chow, C. Y., Foundations of Aerodynamics, John Wiley and Sons, Inc., 1976.
30. Lorber, P. F., and Franklin, C. O., "Airfoil Dynamic Stall at Constant Pitch Rate and High Reynolds Number", AIAA Paper Number AIAA-87-1329, June 1987.
31. Ball, R. E., The Fundamentals of Aircraft Survivability Analysis and Design, AIAA Education Series, AIAA Inc., 1985.

APPENDIX A

Vehicle Drag Polar Development

This Appendix describes the methods used to obtain a drag polar for the baseline vehicle described in Figure 2.2 of Chapter 2. The methods used to develop the drag polar were obtained from Nicolai [20:Chap 11].

The total drag of the vehicle can be expressed as :

$$C_D = C_{D_0} + K C_L^2 \quad (A.1)$$

where :

$$C_{D_0} = C_{D_0 \text{ BD}} + C_{D_0 \text{ wing}} + C_{D_0 \text{ interf}} + C_{D_0 \text{ trim}} + C_{D_0 \text{ vt+nt}} \quad (A.2)$$

For subsonic conditions, $C_{D_0 \text{ BD}}$ is essentially skin friction drag and can be expressed as :

$$C_{D_0 \text{ BD}} = C_{D_f \text{ BD}} + C_{D_{\text{base}}} \quad (A.3)$$

where :

$$C_{D_f BD} = C_f [1 + 60 / (l_{BD} / d)^3 + 0.0025 (l_{BD} / d)] (S_s / S_{BD}) \quad (A.4)$$

and :

$$C_{D_{base}} = 0.029 C_f^{\frac{1}{2}} (d_{base} / d)^3 \quad (A.5)$$

The turbulent flat plate skin friction coefficient for the body, C_f , is found in Figure E.2 of Nicolai by assuming an equivalent sand roughness, k , of 0.4×10^{-3} inches for an average application of standard camouflage paint. The Reynold's number based on body length, $R l_{BD}$, is $5. \times 10^7$ for $M_0 = 0.5$ vehicle. S_s is the total wetted area of the body. $C_{D_0 BD}$ in Equation A.3 is based upon the maximum cross-sectional area of the body, S_{BD} .

The drag coefficient for the wing, $C_{D_0 wing}$, is also mostly skin friction and can be expressed as :

$$C_{D_0 wing} = C_f [1 + L_p (t/c) + 100(t/c)^4] (R S_{wetw} / S) \quad (A.6)$$

where S_{wetw} is the wetted area of the wing and t/c is .15 for the 0015 airfoil. C_f for the wing is found in the same manner as for the body. R is the lifting surface correlation factor found in Figure 11.8 of Nicolai and L_p is the airfoil thickness location parameter. Similarly, the drag coefficient for the vertical and horizontal tail, $C_{D_0 \text{ vt+ht}}$, is found using the methods described for the wing.

No direct estimate of interference drag coefficient, $C_{D_0 \text{ interf}}$, or trim drag coefficient, $C_{D_0 \text{ trim}}$, was made for this vehicle. Based on Hoerner [26] the following values are assumed :

$$C_{D_0 \text{ interf}} = 0.05 C_{D_0} \quad (\text{A.7})$$

$$C_{D_0 \text{ trim}} = 0.10 C_{D_0} \quad \text{A.8}$$

Returning to Equation A.1, the drag due to lift factor, K , can be described as :

$$K = K' + K''$$

where K'' is the viscous drag due to lift.

10-8190 497

PERFORMANCE OPTIMIZATION OF A CRUISE MISSILE USING
DYNAMIC-STALL INDUCED. (U) AIR FORCE INST OF TECH
WRIGHT-PATTERSON AFB OH SCHOOL OF ENGI.. W J DARDIS

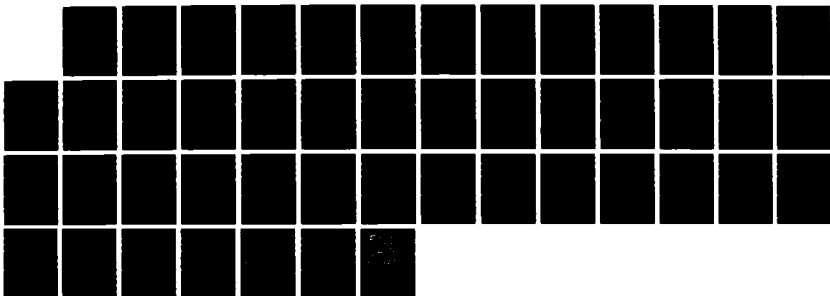
2/2

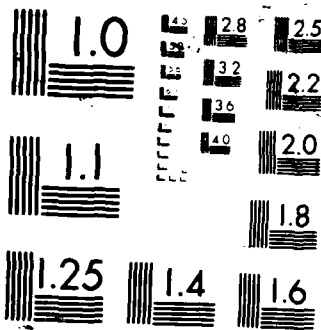
UNCLASSIFIED

SEP 87 AFIT/GAE/RA/875-1

F/G 16/2.1

NL





11.6 of Nicolai and K' is the inviscid drag due to lift factor defined by :

$$K' = 1 / \pi AR e \quad (A.10)$$

The wing efficiency factor, e , is defined as :

$$e = e' [1 - (d / b)^2] \quad (A.11)$$

e' is found in Figure 11.5 of Nicolai. Inlet spillage drag, ram drag, and nozzle-afterbody drag are not specifically addressed and are assumed to be part of the engine thrust data presented in Figures 2.3 and 2.4 of Chapter 2.

Solving Equations A.2 through A.11, Equation A.1 becomes :

$$C_D = 0.040828 + 0.0856 C_L^2 \quad (A.12)$$

Equation A.12 is then the drag polar for the baseline vehicle.

Determination of $C_{L_{max}}$

The maximum lift coefficient of a finite wing can be expressed in terms of the section lift coefficient of that wing as :

$$C_{L_{max}} = C_{l_{max}} / [1 + (m_0 / AR)] \quad (A.13)$$

Based upon tabulated data in Abbott and Von Doenhoff [23], the extrapolated value of $C_{l_{max}}$ for a 0015 airfoil is 1.6. Therefore, $C_{L_{max}}$ for the baseline wing is 1.387.

Drag Polar Equations for the Dynamic-Lift Vehicles

The drag polars for the dynamic-lift vehicles are developed by the same methods as were used for the baseline vehicle accounting for the differences in C_{D_0} due to reduced wing areas and the differences in K due to changes in aspect ratio. The equations are :

$$\text{Vehicle 1 : } C_D = 0.032657 + 0.1059731 C_L^2 \quad (A.14)$$

$$\text{Vehicle 2 : } C_D = 0.032620 + 0.0861453 C_L^2 \quad (A.15)$$

$$\text{Vehicle 3 : } C_D = 0.0326389 + 0.0725063 C_L^2 \quad (\text{A.16})$$

Equations A.14 through A.16 are based on the baseline wing reference area of 13 square feet. At maximum dynamic lift, a value of 0.1 times C_{D_0} is added to C_D in the polar to account for any drag penalties associated with the dynamic-lift event.

APPENDIX B

Critical Mach Number Considerations

This Appendix describes the fundamental equations used to compute the freestream critical Mach number, $M_{\infty \text{ crit}}$, for an airfoil with the methods described in Kuethe and Chow [29]. $M_{\infty \text{ crit}}$ can be calculated if the airfoil minimum pressure coefficient, C_p , is known at a lower freestream Mach number, M_{∞} . Pressure and Mach number can be related by the isentropic relationship :

$$\frac{P_x}{P_0} = [1 + \frac{1}{2}(\gamma - 1) M_0^2]^{-\gamma/(1-\gamma)} \quad (B.1)$$

If P_{∞} and M_{∞} are the freestream pressure and Mach number then,

$$\frac{P_x}{P_{\infty}} = \left[\frac{1 + \frac{1}{2}(\gamma - 1) M_x^2}{1 + \frac{1}{2}(\gamma - 1) M_{\infty}^2} \right]^{\gamma / (1 - \gamma)} \quad (B.2)$$

where "x" is a point or location of minimum pressure coefficient on the airfoil surface. The pressure coefficient at a point on the air-

foil where the minimum pressure is observed is,

$$C_{p_x} = (P_x - P_\infty) / \left(\frac{1}{2} \rho_\infty V_\infty^2 \right) \quad (B.3)$$

Substituting Equation B.2 into B.3 :

$$C_{p_x} = \frac{2}{\gamma M_\infty^2} \left\{ \left[\frac{1 + \frac{1}{2}(\gamma - 1) M_x^2}{1 + \frac{1}{2}(\gamma - 1) M_\infty^2} \right]^{1/\gamma} - 1 \right\} \quad (B.4)$$

If M is equal to 1 at the location of minimum pressure coefficient, then $M_\infty = M_\infty \text{ crit}$ and $C_{p_x} = C_{p_x \text{ crit}}$. Therefore Equation B.4 become :

$$C_{p_x} = \frac{2}{\gamma M_\infty^2} \left\{ \left[\frac{\frac{1}{2}(\gamma - 1)}{1 + \frac{1}{2}(\gamma - 1) M_\infty^2 \text{ crit}} \right]^{1/\gamma} - 1 \right\} \quad (B.5)$$

The critical Mach number for a given airfoil can be found by choosing the minimum pressure coefficient from test data at

lower speeds and by applying the Prandtl-Glauert rule :

$$C_p = C_{p1} \left[(1 - M_{\infty 1}^2) / (1 - M_{\infty}^2) \right]^{\frac{1}{2}} \quad (B.6)$$

where C_{p1} and $M_{\infty 1}$ are taken from test data. By cross-plotting Equations B.4 and B.6, the critical Mach number, M_{∞} crit, is found at the point of intersection of these two curves.

For the 0015 airfoil used in this investigation, the largest minimum value of pressure coefficient is found to be -4.7 for an α_{ND} of 0.022, an α of 22.3 degrees, and a V_{∞} of 30.12 ft/sec [12]. Therefore, for this location,

$$C_{p1} = -4.7 \quad (B.7)$$

$$M_{\infty 1} = 0.0268 \quad (B.8)$$

Substituting Equations B.7 and B.8 into Equation B.6 :

$$C_p = -4.7 \left[0.9992721 / (1 - M_{\infty}^2) \right]^{\frac{1}{2}} \quad (B.9)$$

Equations B.4 and B.9 are cross-plotted in Figure B.1.

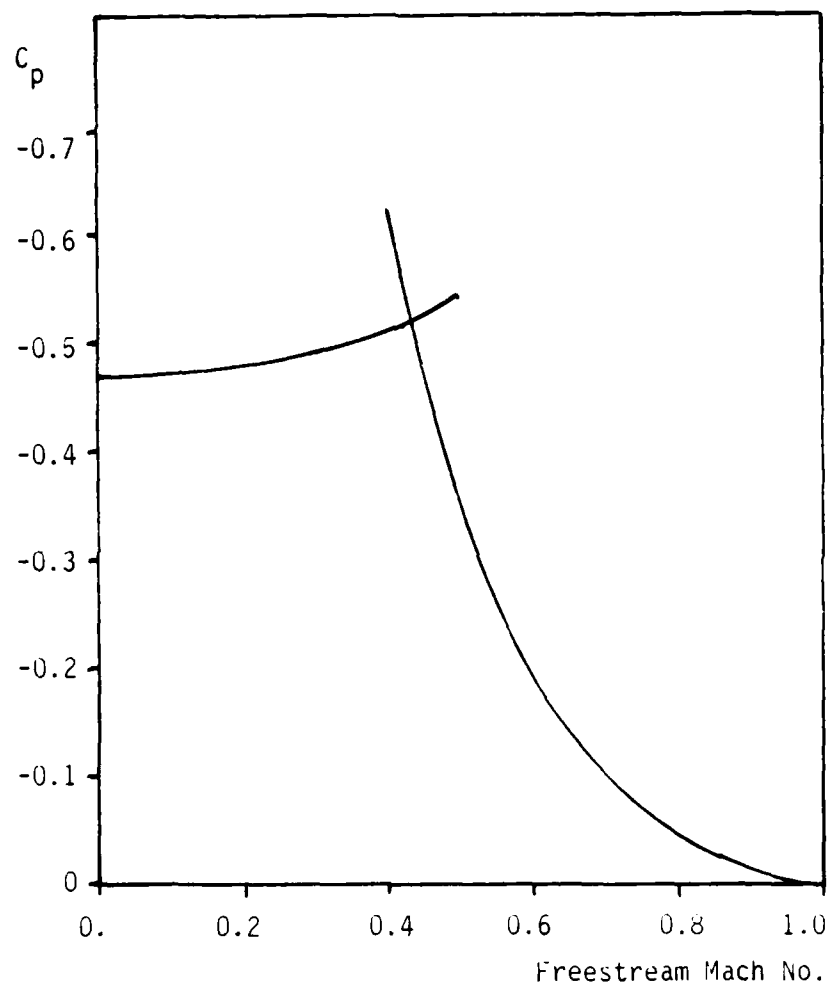


Figure B.1. Critical Mach Number for the
0015 Airfoil During Dynamic Lift
Operation

APPENDIX C

Sample Input and Output for Programs

NSEGII and IIID

94251	0.1339	0.4382	0.4425
94260	0.1360	0.4463	0.4507
94269	0.1467	0.4648	0.4707
94278	0.1495	0.4846	0.4915
94287	0.1513	0.5035	0.5122
94296	0.1559	0.5225	0.5355
94305	0.1623	0.5385	0.5522
94314	0.1676	0.5516	0.5655
94323	0.1732	0.5637	0.5672
94332	0.1799	0.5747	0.5773
94341	0.1857	0.5854	0.5889
94350	0.1913	0.5951	0.5980
94359	0.1969	0.6056	0.6089
94368	0.2027	0.6164	0.6197
94377	0.2082	0.6271	0.6299
94386	0.2138	0.6378	0.6404
94395	0.2195	0.6484	0.6510
94404	0.2251	0.6589	0.6615
94413	0.2307	0.6695	0.6721
94422	0.2363	0.6801	0.6827
94431	0.2419	0.6907	0.6933
94440	0.2475	0.7012	0.7038
94449	0.2531	0.7118	0.7144
94458	0.2587	0.7224	0.7250
94467	0.2643	0.7329	0.7355
94476	0.2699	0.7435	0.7461
94485	0.2755	0.7541	0.7567
94494	0.2811	0.7647	0.7673
94503	0.2867	0.7753	0.7779
94512	0.2923	0.7859	0.7885
94521	0.2979	0.7965	0.8000
94530	0.3035	0.8071	0.8105
94539	0.3091	0.8177	0.8211
94548	0.3147	0.8283	0.8317
94557	0.3123	0.8389	0.8423
94566	0.3179	0.8495	0.8529
94575	0.3235	0.8599	0.8633
94584	0.3291	0.8705	0.8739
94593	0.3347	0.8812	0.8846
94602	0.3393	0.8918	0.8951
94611	0.3449	0.9024	0.9054
94620	0.3495	0.9130	0.9159
94629	0.3551	0.9236	0.9265
94638	0.3607	0.9342	0.9371
94647	0.3663	0.9448	0.9477
94656	0.3719	0.9554	0.9583
94665	0.3775	0.9660	0.9689
94674	0.3831	0.9766	0.9795
94683	0.3887	0.9872	0.9901
94692	0.3943	0.9978	0.9997
94701	0.4000	0.9984	0.9999
94709	0.4056	0.9990	1.0000
94718	0.4112	1.0000	1.0000
94727	0.4168	1.0000	1.0000
94736	0.4224	1.0000	1.0000
94745	0.4280	1.0000	1.0000
94754	0.4336	1.0000	1.0000
94763	0.4392	1.0000	1.0000
94772	0.4448	1.0000	1.0000
94781	0.4504	1.0000	1.0000
94790	0.4560	1.0000	1.0000
94799	0.4616	1.0000	1.0000
94808	0.4672	1.0000	1.0000
94817	0.4728	1.0000	1.0000
94826	0.4784	1.0000	1.0000
94835	0.4840	1.0000	1.0000
94844	0.4896	1.0000	1.0000
94853	0.4952	1.0000	1.0000
94862	0.5008	1.0000	1.0000
94871	0.5064	1.0000	1.0000
94880	0.5120	1.0000	1.0000
94889	0.5176	1.0000	1.0000
94898	0.5232	1.0000	1.0000
94907	0.5288	1.0000	1.0000
94916	0.5344	1.0000	1.0000
94925	0.5399	1.0000	1.0000
94934	0.5455	1.0000	1.0000
94943	0.5511	1.0000	1.0000
94952	0.5567	1.0000	1.0000
94961	0.5623	1.0000	1.0000
94970	0.5679	1.0000	1.0000
94979	0.5735	1.0000	1.0000
94988	0.5791	1.0000	1.0000
94997	0.5847	1.0000	1.0000
95006	0.5893	1.0000	1.0000
95015	0.5949	1.0000	1.0000
95024	0.5955	1.0000	1.0000
95033	0.5961	1.0000	1.0000
95042	0.5967	1.0000	1.0000
95051	0.5973	1.0000	1.0000
95060	0.5979	1.0000	1.0000
95069	0.6035	1.0000	1.0000
95078	0.6091	1.0000	1.0000
95087	0.6147	1.0000	1.0000
95096	0.6193	1.0000	1.0000
95105	0.6249	1.0000	1.0000
95114	0.6295	1.0000	1.0000
95123	0.6351	1.0000	1.0000
95132	0.6407	1.0000	1.0000
95141	0.6463	1.0000	1.0000
95150	0.6519	1.0000	1.0000
95159	0.6575	1.0000	1.0000
95168	0.6631	1.0000	1.0000
95177	0.6687	1.0000	1.0000
95186	0.6743	1.0000	1.0000
95195	0.6799	1.0000	1.0000
95204	0.6855	1.0000	1.0000
95213	0.6911	1.0000	1.0000
95222	0.6967	1.0000	1.0000
95231	0.7023	1.0000	1.0000
95240	0.7079	1.0000	1.0000
95249	0.7135	1.0000	1.0000
95258	0.7191	1.0000	1.0000
95267	0.7247	1.0000	1.0000
95276	0.7293	1.0000	1.0000
95285	0.7349	1.0000	1.0000
95294	0.7395	1.0000	1.0000
95303	0.7451	1.0000	1.0000
95312	0.7507	1.0000	1.0000
95321	0.7563	1.0000	1.0000
95330	0.7619	1.0000	1.0000
95339	0.7675	1.0000	1.0000
95348	0.7731	1.0000	1.0000
95357	0.7787	1.0000	1.0000
95366	0.7843	1.0000	1.0000
95375	0.7899	1.0000	1.0000
95384	0.7955	1.0000	1.0000
95393	0.8011	1.0000	1.0000
95402	0.8067	1.0000	1.0000
95411	0.8123	1.0000	1.0000
95420	0.8179	1.0000	1.0000
95429	0.8235	1.0000	1.0000
95438	0.8291	1.0000	1.0000
95447	0.8347	1.0000	1.0000
95456	0.8393	1.0000	1.0000
95465	0.8449	1.0000	1.0000
95474	0.8495	1.0000	1.0000
95483	0.8551	1.0000	1.0000
95492	0.8607	1.0000	1.0000
95501	0.8663	1.0000	1.0000
95510	0.8719	1.0000	1.0000
95519	0.8775	1.0000	1.0000
95528	0.8831	1.0000	1.0000
95537	0.8887	1.0000	1.0000
95546	0.8943	1.0000	1.0000
95555	0.8999	1.0000	1.0000
95564	0.9055	1.0000	1.0000
95573	0.9111	1.0000	1.0000
95582	0.9167	1.0000	1.0000
95591	0.9223	1.0000	1.0000
95599	0.9279	1.0000	1.0000
95608	0.9335	1.0000	1.0000
95617	0.9391	1.0000	1.0000
95626	0.9447	1.0000	1.0000
95635	0.9493	1.0000	1.0000
95644	0.9549	1.0000	1.0000
95653	0.9595	1.0000	1.0000
95662	0.9651	1.0000	1.0000
95671	0.9707	1.0000	1.0000
95680	0.9763	1.0000	1.0000
95689	0.9819	1.0000	1.0000
95698	0.9875	1.0000	1.0000
95707	0.9931	1.0000	1.0000
95716	0.9987	1.0000	1.0000
95725	0.9995	1.0000	1.0000
95734	0.9999	1.0000	1.0000
95743	1.0000	1.0000	1.0000

DEER HORN 111-5555-3100, 111-5555-3101, 111-5555-3102

86/86/

卷之三

47014- 3.
47MB01- 0...10000.
-30. .50 .70.
5315. 330

四

c.3

LITERATURE

卷之三

END MISSION
END RUN
END OF FILE

0.5

MISSION SEGMENT TABLE

INSEGII SAMPLE OUTPUT

MISSION TIME HISTORY									
WEIGHT		MACH		ALTITUDE		INCREMENTAL RANGE (MARS)		TIME (HRS)	
3000.	.5000	0.	.00	0.	.00	0.	.00	0.	.00
1200.	.5000	0.	2411.94	7.298	1800.	2411.94	7.30	1800.	3

MISSION TIME HISTORY									
WEIGHT		MACH		ALTITUDE		INCREMENTAL RANGE (MARS)		TIME (HRS)	
0	IND001=0.	IND002=1.	IND003=1.	IND004=0.	IND005=0.	IND006=0.	IND007=0.	IND008=0.	IND009=0.
	IND010=0.	IND011=0.	IND012=0.	IND013=0.	IND014=0.	IND015=0.	IND016=0.	IND017=0.	IND018=0.
	IND019=0.	IND020=0.	IND021=0.	IND022=0.	IND023=0.	IND024=0.	IND025=0.	IND026=0.	IND027=0.
	IND028=0.	IND029=0.	IND030=0.	IND031=0.	IND032=0.	IND033=0.	IND034=0.	IND035=0.	IND036=0.
	IND037=0.	IND038=0.	IND039=0.	IND040=0.	IND041=0.	IND042=0.	IND043=0.	IND044=0.	IND045=0.

MISSION TIME HISTORY									
WEIGHT		MACH		ALTITUDE		INCREMENTAL RANGE (MARS)		TIME (HRS)	
0	AMTO	MTD	SPOL	FF	RCSC	AMTO	MTD	SPOL	FF
	.5000	.0000	.0000	.0000	.3000	.5000	.0000	.0000	.0000
	TSIZEF=1.0000	SFCFAC=1.0000	CDFAC=1.0000			XOSH=1.0000	NUNENG=1.0000	ANLTH=1.0000	QLTH=2131.0
									RETUGT=1200.
									FUELUS=1300.
									CLMAX=1.3867

END OF FILE READING DATA

12-28-39. FILE USED, STC39.
 12-28-39. USP, E20289.,

12-28-39. MBS, E20289.,
 12-28-40. CHARGE & CHARGE & EXPIRED 87/11/28.
 12-28-40. CHARGE & EXPIRED 88/02/28. E840282

12-28-40. CHARGE & EXPIRED 88/02/28. E840282
 12-28-41. SPECIUS, PPOC1, GETON.
 12-28-44. SETFS, PROC1, FSAD.
 12-28-44. PPU1

12-28-45. NOTE: OUTPUT, NP, + WELCOME TO NOS 2.5.2 L678

BASELINE

STOCHIE TAB512
 MTAB02/464
 MTAB46 200
 MTAB47 200
 MTAB48 200
 MTAB49 200
 MTAB50 200
 MTAB51 200
 MTAB52 200
 TTAB01/53
 TTAB02/505
 MTAB01/500
 MTAB02/500
 ENC
 STOCHIE DUTM1

CDF 81 STD DAY ATMOS
 STD ATMOSPHERE
 ILLUMIN 3, S STANDARD ATMOS

HP 86 STD DAY AERO

TMB01 .. DELY MP86, RN-CORR, STD DAY
 TMB02 .. DECK MP86, PARABOLIC CURVE FIT DRAG MODEL
 CLMTAB .. ILLUM ZARBL, CLMAX, F(M,CG),

RPPU IMPIMBLES
 OSU-13
 (DMU-0, 0,
 UPMS MODELS

INU0400-1,
 1402/154,
 MTAB02/54

Time	0.0	0.1	0.2	0.3	0.4	0.5	0.6	0.7	0.8	0.9	1.0	1.1	1.2	1.3
Altitude	0.0	1.4	2.1	2.8	3.5	4.2	4.9	5.6	6.3	7.0	7.7	8.4	9.1	9.8
Velocity	0.0	0.15	0.22	0.29	0.36	0.43	0.50	0.57	0.63	0.70	0.77	0.84	0.91	0.98
Angle of Attack	0.0	0.16	0.17	0.18	0.19	0.20	0.21	0.22	0.23	0.24	0.25	0.26	0.27	0.28
Angle of Sideslip	0.0	0.05	0.11	0.17	0.23	0.29	0.35	0.41	0.47	0.53	0.59	0.65	0.71	0.77
Vertical Velocity	0.0	0.10	0.17	0.24	0.31	0.38	0.45	0.52	0.59	0.66	0.73	0.80	0.87	0.94
Vertical Acceleration	0.0	0.05	0.11	0.17	0.23	0.29	0.35	0.41	0.47	0.53	0.59	0.65	0.71	0.77
Roll Rate	0.0	0.05	0.11	0.17	0.23	0.29	0.35	0.41	0.47	0.53	0.59	0.65	0.71	0.77
Pitch Rate	0.0	0.05	0.11	0.17	0.23	0.29	0.35	0.41	0.47	0.53	0.59	0.65	0.71	0.77
Yaw Rate	0.0	0.05	0.11	0.17	0.23	0.29	0.35	0.41	0.47	0.53	0.59	0.65	0.71	0.77

1110 SAMPLE INPUT

1.26,	1.27,	1.28,	1.29,	1.30,	1.31,	1.32,
1.33,	1.34,	1.35,	1.36,	1.37,	1.38,	1.39,
1.40,	1.41,	1.42,	1.43,	1.44,	1.45,	1.46,
1.47,	1.48,	1.49,	1.50,	1.51,	1.52,	1.53,
0.9,	9,	9,	9,	9,	9,	9,
0.6982,	0.6984,	0.6986,	0.6988,	0.6990,	0.6992,	0.6994,
0.94125,	0.94138,	0.94152,	0.94166,	0.94180,	0.94194,	0.94207,
0.94251,	0.94275,	0.94302,	0.94329,	0.94356,	0.94382,	0.94407,
0.94460,	0.94497,	0.94536,	0.94576,	0.94618,	0.94661,	0.94707,
0.94754,	0.94803,	0.94833,	0.94865,	0.94959,	0.95015,	0.95072,
0.95131,	0.95192,	0.95155,	0.95319,	0.95385,	0.95552,	0.95521,
0.95593,	0.95666,	0.95749,	0.95857,	0.95947,	0.95747,	0.95555,
0.96138,	0.96223,	0.96319,	0.96397,	0.96427,	0.96579,	0.96572,
0.96767,	0.96864,	0.96942,	0.97063,	0.97164,	0.97258,	0.97373,
0.97489,	0.97589,	0.97619,	0.97812,	0.97925,	0.98041,	0.98158,
0.98227,	0.98398,	0.98529,	0.98644,	0.98779,	0.98898,	0.98927,
0.99158,	0.99291,	0.99325,	0.99561,	0.99699,	0.99739,	0.99800,
1.01231,	1.02677,	1.04144,	1.05612,	1.0712,	1.0963,	1.11016,
1.11171,	1.13288,	1.1486,	1.1616,	1.1808,	1.1972,	1.2127,
1.23041,	1.2472,	1.2663,	1.285,	1.2989,	1.3164,	1.3341,
1.35260,	1.3701,	1.3983,	1.4087,	1.4253,	1.4440,	1.4626,
1.48221,	1.50113,	1.5207,	1.5443,	1.5691,	1.5881,	1.6062,
1.62661,	1.6469,	1.6615,	1.68327,	1.7033,	1.7245,	1.7453,
1.7673,	1.7889,	1.8098,	1.8327,	1.8549,	1.8773,	1.8998,
1.9225,	1.9453,	1.9683,	1.9955,	2.0149,	2.0384,	2.0622,
2.0866,	2.1191,	2.1424,	2.1597,	2.1823,	2.2056,	2.2289,
2.2588,	2.2833,	2.3087,	2.3313,	2.3666,	2.3986,	2.4221,
0.94083,	0.94084,	0.94086,	0.94091,	0.94096,	0.94104,	0.94114,
0.94125,	0.94138,	0.94152,	0.94168,	0.94186,	0.94206,	0.94227,
0.94251,	0.94275,	0.94302,	0.94329,	0.94356,	0.94382,	0.94407,
0.94460,	0.94497,	0.94536,	0.94576,	0.94618,	0.94661,	0.94707,
0.94754,	0.94803,	0.94833,	0.94953,	0.94995,	0.95052,	0.95072,
0.95131,	0.95192,	0.95255,	0.95319,	0.95385,	0.95522,	0.95552,
0.95593,	0.95666,	0.95749,	0.95796,	0.95846,	0.95974,	0.96052,
0.96138,	0.96223,	0.96319,	0.96397,	0.96427,	0.96579,	0.96521,
0.96767,	0.96864,	0.9692,	0.97063,	0.97164,	0.97268,	0.97333,
0.97489,	0.97589,	0.97619,	0.97812,	0.97925,	0.98041,	0.98158,
0.98227,	0.98398,	0.98529,	0.98644,	0.98779,	0.98898,	0.98927,
0.99158,	0.99291,	0.99325,	0.99561,	0.99699,	0.99739,	0.99800,
1.01231,	1.02677,	1.04144,	1.05612,	1.0712,	1.0863,	1.1016,
1.11171,	1.13288,	1.1486,	1.1616,	1.1808,	1.1972,	1.2137,
1.23041,	1.2472,	1.2663,	1.285,	1.2989,	1.3164,	1.3341,
1.35260,	1.3701,	1.3983,	1.4087,	1.4253,	1.4440,	1.4626,
1.48221,	1.50113,	1.5207,	1.5443,	1.5691,	1.5881,	1.6062,
1.62661,	1.6469,	1.6615,	1.68327,	1.7033,	1.7245,	1.7453,
1.7673,	1.7889,	1.8098,	1.8327,	1.8549,	1.8773,	1.8998,
1.9225,	1.9453,	1.9683,	1.9955,	2.0149,	2.0384,	2.0622,
2.0866,	2.1191,	2.1424,	2.1597,	2.1823,	2.2056,	2.2289,
2.2588,	2.2833,	2.3087,	2.3313,	2.3666,	2.3986,	2.4221,

1.9 66 STU LHR PPGP
TT4601 & TT4602 - DEC 1986, MIN-SPEC-ENG, STD-DAY

1.9 66 STU LHR PPGP
TT4601 & TT4602 - DEC 1986, MIN-SPEC-ENG, STD-DAY
SF.C45.1.0.

1.9 66 STU LHR PPGP
TT4601 & TT4602 - DEC 1986, MIN-SPEC-ENG, STD-DAY
SF.C45.1.0.

86 / 86 /

C.10

ENDIM=1.0,
PHINIT=0.0,

DECK GLEVEL TABLE SWITCHES

HUMGLU=2.,

GLVLIB=2.,

INDA45=0.,

IM45=13.,

IM45Y=2.,

IMTAB46=1.,

IMTAB47=1.,

IMTAB48=1.,

IMTAB49=1.,

IMTAB50=1.,

IMTAB51=1.,

IMTAB52=1.,

IMTAB53=1.,

IMTAB54=1.,

IMTAB55=1.,

IMTAB56=1.,

IMTAB57=1.,

IMTAB58=1.,

IMTAB59=1.,

IMTAB60=1.,

IMTAB61=1.,

IMTAB62=1.,

IMTAB63=1.,

IMTAB64=1.,

IMTAB65=1.,

IMTAB66=1.,

IMTAB67=1.,

IMTAB68=1.,

IMTAB69=1.,

IMTAB70=1.,

IMTAB71=1.,

IMTAB72=1.,

IMTAB73=1.,

IMTAB74=1.,

IMTAB75=1.,

IMTAB76=1.,

IMTAB77=1.,

IMTAB78=1.,

IMTAB79=1.,

IMTAB80=1.,

IMTAB81=1.,

IMTAB82=1.,

IMTAB83=1.,

IMTAB84=1.,

IMTAB85=1.,

IMTAB86=1.,

IMTAB87=1.,

29

HUMPHRI=10.,

PHITAB=1.5, -29.2, 0, 0, 116.67, -9.69, -48.4375, 0, 0, 9.18, 0, , 30.,

IMTAB47=0.,

IMTAB48=13.,

IMTAB49=10.,

IMTAB50=7.,

IMTAB51=2.,

IMTAB52=3.,

IMTAB53=4.,

IMTAB54=5.,

IMTAB55=6.,

IMTAB56=7.,

IMTAB57=8.,

IMTAB58=9.,

IMTAB59=10.,

IMTAB60=11.,

IMTAB61=12.,

IMTAB62=13.,

IMTAB63=14.,

IMTAB64=15.,

IMTAB65=16.,

IMTAB66=17.,

IMTAB67=18.,

IMTAB68=19.,

IMTAB69=20.,

IMTAB70=21.,

IMTAB71=22.,

IMTAB72=23.,

IMTAB73=24.,

IMTAB74=25.,

IMTAB75=26.,

IMTAB76=27.,

IMTAB77=28.,

IMTAB78=29.,

IMTAB79=30.,

IMTAB80=31.,

IMTAB81=32.,

IMTAB82=33.,

IMTAB83=34.,

IMTAB84=35.,

IMTAB85=36.,

IMTAB86=37.,

IMTAB87=38.,

HEPU TABLE SWITCHES

HUMPC=4.,

IMTAB42=1., 2.,

IMTAB43=0.,

IMTAB44=1.,

IMTAB45=1.,

IMTAB46=1.,

IMTAB47=1.,

IMTAB48=1.,

IMTAB49=1.,

IMTAB50=1.,

IMTAB51=1.,

IMTAB52=1.,

IMTAB53=1.,

IMTAB54=1.,

IMTAB55=1.,

IMTAB56=1.,

IMTAB57=1.,

IMTAB58=1.,

IMTAB59=1.,

IMTAB60=1.,

IMTAB61=1.,

IMTAB62=1.,

IMTAB63=1.,

IMTAB64=1.,

IMTAB65=1.,

IMTAB66=1.,

IMTAB67=1.,

IMTAB68=1.,

IMTAB69=1.,

IMTAB70=1.,

IMTAB71=1.,

IMTAB72=1.,

IMTAB73=1.,

IMTAB74=1.,

IMTAB75=1.,

IMTAB76=1.,

IMTAB77=1.,

IMTAB78=1.,

IMTAB79=1.,

IMTAB80=1.,

IMTAB81=1.,

IMTAB82=1.,

IMTAB83=1.,

IMTAB84=1.,

IMTAB85=1.,

IMTAB86=1.,

IMTAB87=1.,

EFILE OF FILE
25

TIME	ALTITUDE	GAMMA	UT	APLIM	QLIM	GLIMIT	IPATH	INDIAN	DTIME	CASE	CASEN
0.00	0.0	0.0	300.0	0.9	2131.0	16.0	0	0	PSI	PSI	CL
.10	0.1	0.1	330.0	0.9	598.2	0	0	0	0	0	0
.20	0.2	0.2	330.0	0.9	598.0	0	0	0	0	0	0
.30	0.3	0.3	330.0	0.9	597.8	0	0	0	0	0	0
.40	0.4	0.4	330.0	0.9	597.5	0	0	0	0	0	0
.50	0.5	0.5	330.0	0.9	597.2	0	0	0	0	0	0
.60	0.6	0.6	330.0	0.9	597.0	0	0	0	0	0	0
.70	0.7	0.7	329.8	0.8	596.9	0	0	0	0	0	0
.80	0.8	0.8	329.6	0.8	596.6	0	0	0	0	0	0
.90	0.9	0.9	329.4	0.8	596.3	0	0	0	0	0	0
1.00	1.0	1.0	329.2	0.8	596.0	0	0	0	0	0	0
1.10	1.1	1.1	329.0	0.8	595.7	0	0	0	0	0	0
1.20	1.2	1.2	329.0	0.8	595.4	0	0	0	0	0	0
1.30	1.3	1.3	329.0	0.8	595.1	0	0	0	0	0	0
1.40	1.4	1.4	329.0	0.8	594.8	0	0	0	0	0	0
1.50	1.5	1.5	329.0	0.8	594.5	0	0	0	0	0	0
1.60	1.6	1.6	329.0	0.8	594.2	0	0	0	0	0	0
1.70	1.7	1.7	329.0	0.8	593.9	0	0	0	0	0	0
1.80	1.8	1.8	329.0	0.8	593.6	0	0	0	0	0	0
1.90	1.9	1.9	329.0	0.8	593.3	0	0	0	0	0	0
2.00	2.0	2.0	329.0	0.8	593.0	0	0	0	0	0	0
2.10	2.1	2.1	329.0	0.8	592.7	0	0	0	0	0	0
2.20	2.2	2.2	329.0	0.8	592.4	0	0	0	0	0	0
2.30	2.3	2.3	329.0	0.8	592.1	0	0	0	0	0	0
2.40	2.4	2.4	329.0	0.8	591.8	0	0	0	0	0	0
2.50	2.5	2.5	329.0	0.8	591.5	0	0	0	0	0	0
2.60	2.6	2.6	329.0	0.8	591.2	0	0	0	0	0	0
2.70	2.7	2.7	329.0	0.8	590.9	0	0	0	0	0	0
2.80	2.8	2.8	329.0	0.8	590.6	0	0	0	0	0	0
2.90	2.9	2.9	329.0	0.8	590.3	0	0	0	0	0	0
3.00	3.0	3.0	329.0	0.8	590.0	0	0	0	0	0	0
3.10	3.1	3.1	329.0	0.8	589.7	0	0	0	0	0	0
3.20	3.2	3.2	329.0	0.8	589.4	0	0	0	0	0	0
3.30	3.3	3.3	329.0	0.8	589.1	0	0	0	0	0	0
3.40	3.4	3.4	329.0	0.8	588.8	0	0	0	0	0	0
3.50	3.5	3.5	329.0	0.8	588.5	0	0	0	0	0	0
3.60	3.6	3.6	329.0	0.8	588.2	0	0	0	0	0	0
3.70	3.7	3.7	329.0	0.8	587.9	0	0	0	0	0	0
3.80	3.8	3.8	329.0	0.8	587.6	0	0	0	0	0	0
3.90	3.9	3.9	329.0	0.8	587.3	0	0	0	0	0	0
4.00	4.0	4.0	329.0	0.8	587.0	0	0	0	0	0	0
4.10	4.1	4.1	329.0	0.8	586.7	0	0	0	0	0	0
4.20	4.2	4.2	329.0	0.8	586.4	0	0	0	0	0	0
4.30	4.3	4.3	329.0	0.8	586.1	0	0	0	0	0	0
4.40	4.4	4.4	329.0	0.8	585.8	0	0	0	0	0	0
4.50	4.5	4.5	329.0	0.8	585.5	0	0	0	0	0	0
4.60	4.6	4.6	329.0	0.8	585.2	0	0	0	0	0	0
4.70	4.7	4.7	329.0	0.8	584.9	0	0	0	0	0	0
4.80	4.8	4.8	329.0	0.8	584.6	0	0	0	0	0	0
4.90	4.9	4.9	329.0	0.8	584.3	0	0	0	0	0	0
5.00	5.0	5.0	329.0	0.8	584.0	0	0	0	0	0	0
5.10	5.1	5.1	329.0	0.8	583.7	0	0	0	0	0	0
5.20	5.2	5.2	329.0	0.8	583.4	0	0	0	0	0	0
5.30	5.3	5.3	329.0	0.8	583.1	0	0	0	0	0	0
5.40	5.4	5.4	329.0	0.8	582.8	0	0	0	0	0	0
5.50	5.5	5.5	329.0	0.8	582.5	0	0	0	0	0	0
5.60	5.6	5.6	329.0	0.8	582.2	0	0	0	0	0	0
5.70	5.7	5.7	329.0	0.8	581.9	0	0	0	0	0	0
5.80	5.8	5.8	329.0	0.8	581.6	0	0	0	0	0	0
5.90	5.9	5.9	329.0	0.8	581.3	0	0	0	0	0	0
6.00	6.0	6.0	329.0	0.8	581.0	0	0	0	0	0	0
6.10	6.1	6.1	329.0	0.8	580.7	0	0	0	0	0	0
6.20	6.2	6.2	329.0	0.8	580.4	0	0	0	0	0	0
6.30	6.3	6.3	329.0	0.8	580.1	0	0	0	0	0	0
6.40	6.4	6.4	329.0	0.8	579.8	0	0	0	0	0	0
6.50	6.5	6.5	329.0	0.8	579.5	0	0	0	0	0	0
6.60	6.6	6.6	329.0	0.8	579.2	0	0	0	0	0	0
6.70	6.7	6.7	329.0	0.8	578.9	0	0	0	0	0	0
6.80	6.8	6.8	329.0	0.8	578.6	0	0	0	0	0	0
6.90	6.9	6.9	329.0	0.8	578.3	0	0	0	0	0	0
7.00	7.0	7.0	329.0	0.8	578.0	0	0	0	0	0	0
7.10	7.1	7.1	329.0	0.8	577.7	0	0	0	0	0	0
7.20	7.2	7.2	329.0	0.8	577.4	0	0	0	0	0	0
7.30	7.3	7.3	329.0	0.8	577.1	0	0	0	0	0	0
7.40	7.4	7.4	329.0	0.8	576.8	0	0	0	0	0	0
7.50	7.5	7.5	329.0	0.8	576.5	0	0	0	0	0	0
7.60	7.6	7.6	329.0	0.8	576.2	0	0	0	0	0	0
7.70	7.7	7.7	329.0	0.8	575.9	0	0	0	0	0	0
7.80	7.8	7.8	329.0	0.8	575.6	0	0	0	0	0	0
7.90	7.9	7.9	329.0	0.8	575.3	0	0	0	0	0	0
8.00	8.0	8.0	329.0	0.8	575.0	0	0	0	0	0	0
8.10	8.1	8.1	329.0	0.8	574.7	0	0	0	0	0	0
8.20	8.2	8.2	329.0	0.8	574.4	0	0	0	0	0	0
8.30	8.3	8.3	329.0	0.8	574.1	0	0	0	0	0	0
8.40	8.4	8.4	329.0	0.8	573.8	0	0	0	0	0	0
8.50	8.5	8.5	329.0	0.8	573.5	0	0	0	0	0	0
8.60	8.6	8.6	329.0	0.8	573.2	0	0	0	0	0	0
8.70	8.7	8.7	329.0	0.8	572.9	0	0	0	0	0	0
8.80	8.8	8.8	329.0	0.8	572.6	0	0	0	0	0	0
8.90	8.9	8.9	329.0	0.8	572.3	0	0	0	0	0	0
9.00	9.0	9.0	329.0	0.8	572.0	0	0	0	0	0	0
9.10	9.1	9.1	329.0	0.8	571.7	0	0	0	0	0	0
9.20	9.2	9.2	329.0	0.8	571.4	0	0	0	0	0	0
9.30	9.3	9.3	329.0	0.8	571.1	0	0	0	0	0	0
9.40	9.4	9.4	329.0	0.8	570.8	0	0	0	0	0	0
9.50	9.5	9.5	329.0	0.8	570.5	0	0	0	0	0	0
9.60	9.6	9.6	329.0	0.8	570.2	0	0	0	0	0	0
9.70	9.7	9.7	329.0	0.8	570.0	0	0	0	0	0	0
9.80	9.8	9.8	329.0	0.8	569.7	0	0	0	0	0	0
9.90	9.9	9.9	329.0	0.8	569.4	0	0	0	0	0	0
10.00	10.0	10.0	329.0	0.8	569.1	0	0	0	0	0	0
10.10	10.1	10.1	329.0	0.8	568.8	0	0	0	0	0	0
10.20	10.2	10.2	329.0	0.8	568.5	0	0	0	0	0	0
10.30	10.3	10.3	329.0	0.8	568.2	0	0	0	0	0	0
10.40	10.4	10.4	329.0	0.8	567.9	0	0	0	0	0	0
10.50	10.5	10.5	329.0	0.8	567.6	0	0	0	0	0	0
10.60	10.6	10.6	329.0	0.8	567.3	0	0	0	0	0	0
10.70	10.7	10.7	329.0	0.8	567.0	0	0	0	0	0	0
10.80	10.8	10.8	329.0	0.8	566.7	0	0	0	0	0	0
10.90	10.9	10.9	329.0	0.8	566.4	0	0	0	0	0	0
11.00	11.0	11.0	329.0	0.8	566.1	0	0	0	0	0	0
11.10	11.1	11.1	329.0	0.8	565.8	0	0	0	0	0	0
11.20	11.2	11.2	329.0	0.8	565.5	0	0	0	0	0	0
11.30	11.3	11.3	329.0	0.8	565.2	0	0	0	0	0	0
11.40	11.4	11.4	329.0	0.8	564.9	0	0	0	0	0	0
11.50	11.5	11.5	329.0	0.8	564.6	0	0	0	0	0	0
11.60	11.6	11.6	329.0	0.8	564.3	0	0	0	0	0	0
11.70	11.7	11.7	329.0	0.8	564.0	0	0	0	0	0	0
11.80	11.8	11.8	329.0	0.8	563.7						

APPENDIX D

Remainder of Tabulated Results

Table D.1

Vehicle Range For Mach Number Equal to 0.5 at
Sea Level With the Baseline Engine

MACH NO.	AVG FUEL FLOW (LBM/HR)	AVG SFC (LBM/HR /LBF)	AVG THRUST (LBF)	TOTAL TIME (HRS)	RANGE (NM)	%INCR. IN RANGE
BASE	.50	251.4	.898	280.0	7.30	2412.
VEH. 1	.50	245.9	.943	260.8	7.56	2500. [2345] +3.70 [-2.78]
VEH. 2	.50	233.8	.969	241.3	7.90	2610. [2455] +8.20 [+1.78]
VEH. 3	.50	226.7	.994	228.1	8.11	2679 [2524] +11.10 [+4.64]

[] = 100 LB FUEL PENALTY APPLIED

Table D.2

Vehicle Range Optimized for Cruise Mach Number
at Sea Level With The Baseline Engine

	MACH NO.	AVG FUEL FLOW (LBM/HR)	AVG SFC (LBM/HR /LBF)	AVG THRUST (LBF)	TOTAL TIME (HRS)	RANGE (NM)	%INCR IN RANGE
BASE	.500	251.4	.898	280.0	7.30	2412.	-----
VEH. 1	.564	259.3	.921	281.5	7.07	2638. [2467]	+9.40 [+2.28]
VEH. 2	.565	247.4	.928	266.5	7.38	2757. [2585]	+14.30 [+7.17]
VEH. 3	.566	239.8	.934	256.7	7.59	2840. [2667]	+17.70 [+10.60]

[] = 100 LB FUEL PENALTY APPLIED

Table D.3

Vehicle Range Optimized for Cruise Mach Number
at 10000 ft Altitude With the Baseline Engine

	MACH NO.	AVG FUEL FLOW (LBM/HR)	AVG SFC (LBM/HR /LBF)	AVG THRUST (LBF)	TOTAL TIME (HRS)	RANGE (NM)	%INCR IN RANGE
BASE	.505	246.3	.959	256.8	7.73	2464.	-----
VEH. 1	.502	249.1	.963	258.7	7.90	2520. [2316]	+2.30 [-6.01]
VEH. 2	.501	222.6	.966	230.4	8.62	2750. [2537]	+11.60 [+2.96]
VEH. 3	.501	204.7	.969	211.2	9.27	2957. [2735]	+20.01 [+11.00]

[] = 100 LB FUEL WEIGHT PENALTY APPLIED

Table D.4

Vehicle Range for Optimum Dynamic Vehicle Engine
 Thrust Characteristics at Mach Number Equal to
 0.5 at Sea Level

MACH NO.	Avg Fuel Flow (Lbm/HR)	Avg SFC (Lbm/hr /lbf)	Avg Thrust (lbf)	Total Time (hrs)	Range (nm)	%Incr in Range
BASE	.50	251.4	.898	280.0	7.30	2412. -----
VEH. 1	.50	232.1	.890	260.8	8.04	2657. +10.20 [2528] [+4.80]
VEH. 2	.50	212.8	.882	241.3	8.71	2877. +19.30 [2737] [+13.50]
VEH. 3	.50	200.7	.880	228.1	9.17	3031. +25.60 [2887] [+19.70]

[] = 100 LB FUEL WEIGHT PENALTY APPLIED

Table D.5

Maximum Lift Coefficient Climb at Weight = 3000 lbs

WT = 3000 LBS	BASE	VEH.1	VEH.2	VEH.3
Max Flight Path Angle	24.9	23.6	25.5	26.9
Time (sec)	16.0	15.3	16.0	16.5
<u>Ballistic</u>				
Max Altitude H (ft)	3433.	3197.	3544.	3801.
Downrange Y (ft)	12241.	11900.	12375.	12612.
Time (sec)	29.9	29.2	30.1	30.8

Table D.6

Maximum Lift Coefficient Climb at Weight = 2000 lbs

WT = 2000 LBS	BASE	VEH.1	VEH.2	VEH.3
Max Flight Path Angle	57.0	54.8	58.5	62.0
Time (sec)	16.4	15.9	16.8	17.4
<u>Ballistic</u>				
Max Altitude H (ft)	4967.	4913.	5071.	5310.
Downrange Y (ft)	7057.	7328.	7011.	6880.
Time (sec)	26.4	26.0	26.6	27.0

Table D.7

Maximum Lift Coefficient Climb at Weight = 1000 lbs

WT = 1000 LBS	BASE	VEH.1	VEH.2	VEH.3
Max Flight Path Angle	90.0	90.0	90.0	90.0
Time (sec)	6.98	7.07	6.86	6.78
<u>At max = 90</u>				
Max Altitude H (ft)	2180.	2212.	2174.	2170.
Downrange Y (ft)	2182.	2215.	2179.	2170.
Time (sec)	6.98	7.07	6.86	6.78

Table D.8

Pull Out of Dive Maneuver for All Four Vehicles at
Weight = 3000 lbs

γ_i	=	INITIAL ALTITUDE / TOTAL TIME			
		-90°	-45°	-30°	-15°
BASELINE		7582.0	2830.3	1437.7	407.24
		16.50	12.25	9.49	5.55
VEH. 1		7613.9	2849.5	1449.0	409.90
		17.10	12.30	9.60	5.61
VEH. 2		7563.8	2821.4	1432.7	406.10
		17.00	12.00	9.40	5.50
VEH. 3		7541.2	2801.1	1422.2	403.60
		16.50	11.50	9.20	5.44

Table D.9

Pull out of Dive Maneuver for All Four Vehicles at
Weight = 2000 lbs

γ_i	=	INITIAL ALTITUDE / TOTAL TIME			
		-90°	-45°	-30°	-15°
BASELINE		5016.5 12.35	1584.1 7.51	746.8 5.27	195.1 2.73
VEH. 1		4640.8 11.57	1522.2 7.10	737.2 5.20	195.1 2.71
VEH. 2		4617.5 11.20	1513.4 7.13	733.1 5.07	194.4 2.70
VEH. 3		4604.6 11.00	1506.9 7.01	730.5 5.00	193.9 2.65

Table D.10

Pull Out of Dive Maneuver for all Four Vehicles at
Weight = 1000 lbs

γ_i	INITIAL ALTITUDE / TOTAL TIME			
	-90°	-45°	-30°	-15°
BASELINE	2384.7 6.21	622.3 3.45	284.1 2.12	73.8 1.07
VEH. 1	1979.6 5.61	550.7 3.10	271.6 2.11	72.6 1.06
VEH. 2	1972.3 5.51	548.6 3.06	271.0 2.11	72.5 1.05
VEH. 3	1966.2 5.50	547.0 3.00	266.8 2.06	72.4 1.01

Table D.11

Effect of Thrust on Pull-Over Capability for a
 Vehicle Weight of 3000 lbs at $\gamma = -90^\circ$,
 and an Initial Mach Number of 0.0

MAX THRUST	ALT (ft)	DOWNRANGE (ft)	TIME (sec)
BASELINE	9081.	8600.	30.4
VEHICLE 1	4135.	5640.	31.7
VEHICLE 2	4056.	5525.	30.1
VEHICLE 3	3002.	5460.	29.8
50% THRUST			
BASELINE	9324.	8860.	31.8
VEHICLE 1	4388.	8962.	32.2
VEHICLE 2	4295.	8791.	31.6
VEHICLE 3	4235.	8680.	31.2

Table D.12

Mission 1 - Baseline Vehicle Traversing the
First Mountain

SEGMENT DESCRIPTION	t(sec)	H(ft)	Mach	Y(nm)
1. Max lift climb to $\gamma = 15^\circ$	4.63	349.	.4738	.410
2. Const climb $\gamma = 15^\circ$	12.00	1907.	.4084	.936
3. Max negative lift pull over to $\gamma = -15^\circ$	4.24	1893.	.4150	.311
4. Level down to :	12.01	278.	.5251	.998
5. Pull-out to level	3.71	0.	.5269	.355
TOTAL TIME = 36.69 sec PRESHOOT = .210 nm OVERSHOOT = .343 nm MAX H = 2028 ft				

Table D.13

Mission 1 - Vehicle 1 Traversing the First
Mountain

SEGMENT DESCRIPTION	t(sec)	H(ft)	Mach	Y(nm)
1. Max Dyn. lift climb to $\gamma = 31.6^\circ$	14.80	2300.	.3448	1.100
2. Negative Dyn lift impulse to $\gamma = 28.8^\circ$.33	2355.	.2575	.015
3. Down to level	32.55	0.	.4556	1.886
TOTAL TIME = 47.68 sec PRESHOOT = .211 nm OVERSHOOT = .333 nm MAX H = 2974 ft				

Table D.14

Mission 1 - Vehicle 2 Traversing the First
Mountain

SEGMENT DESCRIPTION	t(sec)	H(ft)	Mach	Y(nm)
1. Max Dyn lift climb to $\gamma = 33.2^\circ$	15.80	2584.	.3412	1.168
2. Max Dyn lift impulse to $\gamma = 29.25^\circ$.47	2660.	.2421	.021
3. Max Dyn lift to level	31.38	0.	.4706	1.846
TOTAL TIME = 47.65 sec PRESHOOT = .208 nm OVERSHOOT = .370 nm MAX H = 3070 ft				

Table D.15

Mission 1 - Vehicle 3 Traversing the First Mountain

SEGMENT DESCRIPTION	t(sec)	H(ft)	Mach	Y(nm)
1. Max Dyn lift climb to $\gamma = 34.4^\circ$	16.00	2693.	.3452	1.188
2. Max negative Dyn lift impulse to $\gamma = 28.4^\circ$.71	2808.	.2306	.031
3. Max Dyn lift to level	30.82	0.	.4815	1.806
TOTAL TIME = 47.53 sec PRESHOOT = .207 nm OVERSHOOT = .361 nm MAX H = 3156 ft				

Table D.16

Mission 1 - Fuel Loss Estimate For the Terrain
Following Portion of the Mission

	WT. AT START OF TERRAIN FOLLOW (LBS)	FUEL USED ABOVE TER (LBS)	FUEL USED BETWEEN TER. (LBS)	WT. AT END OF TERRAIN FOLLOW (LBS)
BASELINE	2621.00	22.10	21.79	2577.11
VEHICLE 1	2639.00	23.50	21.82	2593.70
VEHICLE 2	2670.00	24.10	21.67	2624.20
VEHICLE 3	2689.00	23.90	21.73	2643.40

Table D.17

Mission 2 - Baseline Vehicle Traversing the
First Mountain

SEGMENT DESCRIPTION	t(sec)	H(ft)	Mach	Y(nm)
1. Const. 1.29g climb	44.98	6010.	.1940	2.970
2. Max neg. lift pull-over to $\gamma = -45^\circ$	5.10	5466.	.2789	.183
3. level down at $\gamma = -45^\circ$	11.80	1536.	.5624	.632
4. Pull-out to level	6.24	0.	.5846	.598
TOTAL TIME = 68.12 sec PRESHOOT = 2.01 nm OVERSHOOT = .398 nm				

Table D.18
Mission 2 - Vehicle 1 Traversing the First
Mountain

SEGMENT DESCRIPTION	t(sec)	H(ft)	Mach	Y(nm)
1. Const 1.251g climb to $\gamma = 22.0^\circ$	23.90	2344.	.4435	2.122
2. Turn on Dyn lift to $\gamma = 0^\circ$	21.22	6002.	.1806	.910
3. Static neg max lift pull-over to $\gamma = -45^\circ$	4.60	5571.	.2679	.180
4. $\gamma = -45^\circ$ down	12.20	1531.	.5471	.641
5. Pull-out to level	6.20	1591.	.5791	.596
TOTAL TIME = 70.12 sec PRESHOOT = 2.052 nm OVERSHOOT = .422 nm				

Table D.19
Mission 2 - Vehicle 2 Traversing the First
Mountain

SEGMENT DESCRIPTION	t(sec)	H(ft)	Mach	Y(nm)
1. Const 1.263g climb to $\gamma = 21.8^\circ$	23.10	2320.	.4421	2.011
2. Turn on Dyn lift to $\gamma = 0^\circ$	21.01	6012.	.1789	.901
3. Static neg. max lift to $\gamma = -45^\circ$	5.20	5390.	.2814	.181
4. $\gamma = -45^\circ$ down	10.84	1521.	.5798	.639
5. Pull-out to level	6.22	0.	.5889	.598
TOTAL TIME = 66.46 sec PRESHOOT = 1.932 nm OVERSHOOT = .423 nm				

Table D.20

Mission 2 - Vehicle 3 Traversing the First
Mountain

SEGMENT DESCRIPTION	t(sec)	H(ft)	Mach	Y(nm)
1. Const 1.279g climb to $\gamma = 21.1^\circ$	22.61	2289.	.4402	1.989
2. Turn on Dyn lift to $\gamma = 0^\circ$	20.34	6008.	.1796	.894
3. Static neg. max lift pull-over to $\gamma = -45^\circ$	5.31	5309.	.2899	.187
4. $\gamma = -45^\circ$ down	10.16	1516.	.5821	.642
5. Pull-out to level	6.18	0.	.5960	.614
TOTAL TIME = 64.60 sec				
PRESHOOT = 1.903 nm				
OVERSHOOT = .431 nm				

Table D.21

Mission 2 - Fuel Loss Estimate For the Terrain
Following Portion of the Mission

	WT. AT START OF TERRAIN FOLLOW (LBS)	FUEL USED ABOVE TER. (LBS)	FUEL USED BETWEEN TER. (LBS)	WT. AT END OF TERRAIN FOLLOW (LBS)
BASELINE	2001.00	64.8	0.83	1935.37
VEHICLE 1	2025.00	64.9	4.73	1955.38
VEHICLE 2	2089.00	62.6	5.19	2020.60
VEHICLE 3	2131.00	60.9	5.95	2064.20

VITA

William J. Dardis III was born on 22 November 1956 in Stamford, Connecticut. He grew up in Stamford and upon graduation from Stamford High School in 1974, attended The Pennsylvania State University in University Park, Pennsylvania. He graduated from Penn State in 1980 with a Bachelor of Science Degree in Aerospace Engineering. After graduation, he began employment at the Aeronautical Systems Division, USAF, Wright-Patterson AFB as internal aerodynamicist for the Aerodynamics and Performance Branch of the Directorate of Flight Systems Engineering where in June of 1985 he entered the School of Engineering, Air Force Institute of Technology.

Permanent Address: 3728 Country Lane
Beavercreek, OH 45430

REPORT DOCUMENTATION PAGE

Form Approved
OMB No. 0704-0188

1a. REPORT SECURITY CLASSIFICATION UNCLASSIFIED		1b. RESTRICTIVE MARKINGS A.D-A190487												
2a. SECURITY CLASSIFICATION AUTHORITY		3. DISTRIBUTION/AVAILABILITY OF REPORT Approved for public release; distribution unlimited.												
2b. DECLASSIFICATION/DOWNGRADING SCHEDULE														
4. PERFORMING ORGANIZATION REPORT NUMBER(S) AFIT/GAE/AA/875-1		5. MONITORING ORGANIZATION REPORT NUMBER(S)												
6a. NAME OF PERFORMING ORGANIZATION School of Engineering	6b. OFFICE SYMBOL (if applicable) AFIT/ENG	7a. NAME OF MONITORING ORGANIZATION												
6c. ADDRESS (City, State, and ZIP Code) Air Force Institute of Technology Wright-Patterson AFB OH 45433		7b. ADDRESS (City, State, and ZIP Code)												
8a. NAME OF FUNDING/SPONSORING ORGANIZATION	8b. OFFICE SYMBOL (if applicable)	9. PROCUREMENT INSTRUMENT IDENTIFICATION NUMBER												
8c. ADDRESS (City, State, and ZIP Code)		10. SOURCE OF FUNDING NUMBERS												
		PROGRAM ELEMENT NO.	PROJECT NO.	TASK NO.	WORK UNIT ACCESSION NO.									
11. TITLE (Include Security Classification) PERFORMANCE OPTIMIZATION OF A CRUISE MISSILE USING DYNAMIC-STALL INDUCED LIFT AUGMENTATION														
12. PERSONAL AUTHOR(S) William J. Dardis III, B.S.														
13a. TYPE OF REPORT Thesis	13b. TIME COVERED FROM _____ TO _____	14. DATE OF REPORT (Year, Month, Day) 1987 September		15. PAGE COUNT 139										
16. SUPPLEMENTARY NOTATION <i>Approved for public release: IAW AFIR 190487. Lynn E. Wolaver 29 Oct 87 Dean for Research and Professional Development AFIT/GAE/AA/875-1</i>														
17. COSATI CODES <table border="1"><tr><th>FIELD</th><th>GROUP</th><th>SUB-GROUP</th></tr><tr><td>20</td><td>04</td><td></td></tr><tr><td></td><td></td><td></td></tr></table>		FIELD	GROUP	SUB-GROUP	20	04					18. SUBJECT TERMS (Continue on reverse if necessary and identify by block number) Stall, Dynamic Stall, Performance Cruise-Missile-Type Aircraft, Range			
FIELD	GROUP	SUB-GROUP												
20	04													
19. ABSTRACT (Continue on reverse if necessary and identify by block number) TITLE: Performance Optimization of a Cruise Missile Using Dynamic-Stall Induced Lift Augmentation THESIS ADVISOR: Eric J. Jumper, Lt Col, USAF														
An investigation was conducted to study the possible performance benefits of using the augmented lift produced by dynamic-stall-type airfoil motions to a cruise-missile-type aircraft in terms of range, climb capability, and susceptibility to threat. A baseline cruise-missile-type aircraft is defined and compared to three modified versions with augmented lift capability. The wings for the three dynamic-lift vehicles are sized to produce the same maximum lift coefficient, while operating dynamically, as the maximum usable lift coefficient (0.8 times maximum lift coefficient) of the baseline aircraft. By resizing the wing through chord reduction, increases in straight-and-level range of 20 to 25% are found along with improvements in climb, pull over terrain, and pull up														
20. DISTRIBUTION/AVAILABILITY OF ABSTRACT <input checked="" type="checkbox"/> UNCLASSIFIED/UNLIMITED <input type="checkbox"/> SAME AS RPT <input type="checkbox"/> DTIC USERS		21. ABSTRACT SECURITY CLASSIFICATION UNCLASSIFIED												
22a. NAME OF RESPONSIBLE INDIVIDUAL L. Hudson, Maj, USAF		22b. TELEPHONE (Include Area Code) (513)255-2998		22c. OFFICE SYMBOL AFIT/ENY										

19. ABSTRACT (CONT'D): from a dive, capability.

Moderate improvements in performance are found for the same aspect ratio vehicle. The vehicle resized by span reduction consistently under-performed all vehicles except in some examples of pull out to level flight. Two typical cruise-missile-type missions were chosen and the trajectories of the four vehicles were modeled. Minimum time above a reference altitude was determined for the two missions as a representative measure of susceptibility to threat.

END
DATE
FILED

4-88

DTIC